Development of a Control and Monitoring Platform Based on Fuzzy Logic for Wind Turbine Gearboxes

A thesis submitted to
the Faculty of Graduate and Postdoctoral Studies
in partial fulfillment of the requirements for the
degree of Master of Applied Science in
Mechanical Engineering

by
Wei Chen

Ottawa-Carleton Institute for Mechanical and Aerospace Engineering
University of Ottawa
Ottawa, Ontario, Canada, K1N 6N5
December 2012

Abstract

It is preferable that control and bearing condition monitoring are integrated, as the condition of the system should influence control actions. As wind turbines mainly work in remote areas, it becomes necessary to develop a wireless platform for the control system.

A fuzzy system with self-tuning mechanism was developed. The input speed error and speed change were selected to control the shaft speed, while the kurtosis and peak-to-peak values were used as another set of inputs to monitor the bearing conditions. To enhance effectiveness, wait-and-see (WAS) logic was used as the pre-processing step for the raw vibration signal.

The system was implemented on the LabVIEW platform. Experiments have shown that the system can effectively adjust motor rotating speed in response to bearing conditions.

For future studies, more advanced fault detection methods can be integrated with proper tuning mechanisms to enrich the performance and function of the controller.

Acknowledgments

I would like to acknowledge my supervisor, Dr. M. Liang, and Dr. C. Li, for their support and detailed guidance throughout. This thesis was a project initiated by the aforementioned and was developed based on their proposal.

I am also grateful for the help of other graduate students at Dr. Liang's lab at the University of Ottawa. Technical assistance from the machine shop of the Department of Mechanical Engineering is also highly appreciated.

Table of Contents

List of Figures

List of Tables

Nomenclature

$C(i)$	Change of speed
C_p	Mean value for maximum membership function
cu	Scaled output voltage change
$c\omega$	Scaled speed change
$E(i)$	Error of speed
$e\omega$	The scaled speed error
i	Sampling period of ω
k	Coefficient for determining the self-tuning mechanism
Kc	Scaling factor for the speed change
Ke	Scaling factor for the speed error
K_u	Scaling factor for voltage change
L_m	The amplitude of mth fault impulse
M	Half of the number of the fault generated impulses
p	The number of relevant rules
$PPV(n)$	The nth input peak-to-peak value
$PPV_{mean}(n)$	Mean value of peak-to-peak values prior to the nth input
T_p	The time period corresponding to the fault characteristic frequency
u	The crisp output
$u(t)$	Unit step function
β	The decay parameter
Δu	Change of voltage
$\Delta(n)$	Difference between $PPV(n)$ and $PPV_{mean}(n)$
μ_p	Membership degree
$\xi(t)$	The expected value of the quantity t
τ_i	The effect of random slippage of the rollers
ω	Real speed of the shaft
ω_{max}	Maximum shaft speed
ω_{min}	Minimum shaft speed

ω_r	The excited resonance frequency
ω_{ref}	Reference speed

Chapter 1. Introduction

1.1 Background

Many wind turbines are subjected to harsh working conditions. Bearing is one of the most important yet failure-prone components in a wind turbine. Control and condition monitoring are vital to wind turbine function and productivity.

Most previous studies on the subject treat the two issues separately. However, control and condition monitoring share much of the same sensing devices and data. Control actions are often affected by gearbox conditions, whereas control data has the potential to benefit monitoring decisions. It is therefore highly desirable to develop a system that can perform both control and monitoring tasks simultaneously.

In addition, it is also important to implement such a system wirelessly because of the remote locations of many wind turbines. The purpose of this study is therefore to develop a wireless control and fault monitoring system for wind turbines.

1.2 Proposed Study

A fuzzy system with self-tuning mechanism is proposed for concurrent control and monitoring because of its tolerance for imprecision of data, uncertainty of the process, and partial truth of prior knowledge, as well as its ability to model non-linear functions of arbitrary complexity and to make use of the experience of domain experts.

This study aims to develop a wireless system for both the control and monitoring of a gearbox to be implemented in a wind turbine system. Specific aims of the study are as follows:

1. To develop a wired control system for the wind turbine device

To control the gearbox speed, both the speed error and the speed change will be used as inputs to the fuzzy controller.

2. To integrate a bearing condition monitoring mechanism into the control system

To monitor gearbox condition, kurtosis and peak-to-peak values will be adopted as another set of inputs to the system. To enhance the effectiveness of input kurtosis values and peak-to-peak values, wait-and-see (WAS) logic will be used to pre-process the raw vibration signal.

3. To develop a wireless platform in implementing the control and monitoring system

A wireless platform based on micro-controller modules will be developed and embedded into the original wired system.

1.3 Contribution of the Study

Generally, control system and monitoring system are developed and operate independently. In this study, a shaft speed control algorithm is developed with consideration of faulty bearings vibration signals. The shaft speed can be adjusted according to the bearing working conditions, i.e., the speed can be slowed down or decreased to zero in response to the bearing fault severity.

1.4 Organization of the Thesis

This thesis is composed of five chapters, including this chapter which gives an introduction to the study. Chapter 2 presents a brief review of previous work pertinent to speed control, self-tuning of fuzzy logic control, and bearing fault detection. The design of the fuzzy logic based control and monitoring platform is detailed in Chapter 3. Chapter 4 illustrates the experimental work to test the proposed control and monitoring platform. The experimental results are also examined in this chapter. In

Chapter 5, conclusions of the study are made, and some topics for further work are suggested.

Chapter 2. Literature Review

Wind energy is one of the several clean energy resources. With the increase in size and height of wind turbines, their maintenance and inspection are becoming increasingly challenging (Ciang *et al* 2008).

Rolling bearings are among the most important components in the wind turbine.Rolling element bearings are among the most common causes of rotating machinery failures (Elforjani and Mba 2010). During the operations, bearings may experience vibrations from many sources such as radial or axial load unbalance, even if the bearings themselves are perfectly healthy. As a bearing fault develops, the vibration becomes more severe (Marichal *et al* 2011) due to the periodic impact when the faulty and normal bearing surfaces are in contact. Therefore, the occurrence of faults can be detected by processing vibration signals from the accelerometer.

Extensive studies have been conducted in either control systems or monitoring systems. In this study, the monitoring action is integrated with the control system in order to detect faults and accordingly slow down or shut down the wind turbine to protect the equipment before further maintenance. The control and monitoring components are integrated based on fuzzy logic mechanism. In real life applications, remote control of the wind turbine is required. Hence, a wireless platform will be developed for this purpose.

2.1 Review of Speed Control Methods

Due to various loads added onto the wind turbine, rotating speed of the wind turbine may change in an undesirable manner. Therefore, it is necessary to develop an efficient controller in order to maintain the rotating speed at a desired value.

Fuzzy logic control method, as compared to traditional control methods, is a good

approach to many complex nonlinear systems or even non-analytic ones, including manufacturing (Precup and Hellendoorn 2011), financial analysis (Smimou *et al* 2008), and economic applications (Díaz *et al* 2006). In the engineering fields, fuzzy control has been widely applied, e.g., for robot arm control (Anh and Ahn 2011), induction motor control (Barazane *et al* 2009, Saad and Arrofiq 2012, Dandil 2009), etc. Fuzzy control has also been employed for wind turbine control such as the controller for speed control (Bououden *et al* 2012), pitch-angle control (Senjyu *et al* 2008, Qi and Meng 2012), power control (Xiao 2010), as well as system control (Dadone and Dambrosio 2003).

The performance of traditional control methods is rarely satisfactory when applied to regulate the speed of devices or machines with nonlinear characteristics or strong coupling features (Li and Liu 2011). A new hybrid control algorithm utilizing recurrent wavelet neural network (RWNN) was proposed by Li and Liu (2011), which can adjust parameters on line in accordance with load disturbance. This method takes advantage of the learning ability of artificial neural networks and the identification ability of wavelet decomposition. Performance of this technique under experimentation has shown that the requirements of fast response and good stability can be satisfied (Li and Liu 2011).Therefore, the learning-based self-adaptive and self-tuning control techniques will be explored in this thesis.

2.1.1 Fuzzy logic based tuning methods

Parameter tuning methods are often proposed based on fuzzy logic rules. Many different tuning methods have been developed.

The proportional-integral-derivative (PID) control method is a popular technique for variable speed motor drive control. However, PID controllers are linear in nature and may not perform well for non-linear systems. In addition, they are prone to noise and measurement errors because the derivative part of such systems tends to yield large

output changes in response to noise. As such, the PID controllers can lead to undesirable control characteristics including larger overshoot, slower settling time, and even instability (Shin and Park 2012). To resolve this problem, PID control with integral state prediction (Shin and Park 2012) was proposed, and the relationship between parameters for examining the performance of the controller and its factors were examined, which enabled further improvement based on this proposed method.

The performances of conventional PID controllers, fuzzy PID controller, and adaptive fuzzy PID controller were compared in a study by Kandiban and Arulmozhiyal (2012). With the conventional PID controller, tuning of parameters is not convenient and the result of control interventions is not satisfactory. In comparison, adaptive fuzzy logic method is easy for computation and allows further development of tuning mechanisms (Kandiban and Arulmozhiyal 2012).

To control the speed, speed change and changes in speed error are used as inputs to the proposed controller in a study conducted by Kandiban and Arulmozhiyal (2012). The adaptive fuzzy controller was adopted to optimize the three coefficients of the PID controller.

In a study conducted by Subramanyam *et al* (2012), a method for determining the proportional, integral, and derivative parameters of a turbine speed control system was proposed. This method was based on the approximation of feedback of internal model control, and it was demonstrated that the performance and robustness of the controller can be efficiently adjusted. Conventional tuning methods such as Ziegler-Nicholas rules and another method developed by Lee *et al* (2006) were discussed in this study, and the latter proved to be robust when applied to internal model control for the PID controller.

Fuzzy adaptive PID controllers were also applied to a semi-active suspension system

on high-speed trains. Both passive suspension and semi-active suspension simulation were conducted based on fuzzy adaptive PID control. Simulation results concluded that the stability of high-speed vehicles can be enhanced by adopting the semi-active suspension proposed in the study by Yang *et al* (2011).

Self-adaptive control was also implemented in numerical control of machining processes to improve productivity. A method dependent on a discrete mathematic model that was based on Z-transform and PID control was proposed to control the feed velocity of the machine by Zhang *et al* (2006). Self-tuning mechanism for PID parameters was designed using the neural network technique. Their experimental results indicated that this method had led to robust performance without complex mathematical modeling.

A continuous action reinforcement learning automaton was proposed by Howell and Best (2000) as a tuning technique. Their experiment showed that this tuning method could facilitate the optimization of the PID parameters for idle-speed control of an engine. In addition, it does not need prior knowledge as required by many other learning algorithms.

Tan *et al* (2001) proposed an approach for PID parameter tuning based on automatic identification of PID configuration and parameters. An automatic tuning mechanism was also developed based on auto-tuning neurons for multivariable systems by Chang *et al* (2003).

2.1.2 Fuzzy rule-base tuning mechanism

In traditional fuzzy logic controllers, fuzzy rule bases are set to fixed values. However, as many systems are dynamic in nature. It is desirable to incorporate some tuning mechanisms to enhance the performance of controllers. A few studies were carried out to improve the accuracy of fuzzy rule-based systems (e.g., Sanz *et al* 2010, Alcala

et al 2007, Sanz *et al* 2011, Sanz *et al* 2010, and Casillas *et al* 2005).

Fine tuning method and function based tuning mechanism were proposed by researchers. For example, the fine tuning method proposed by Gürocak and Lazaro (1994) can tune the rule bases by adjustment of the points of maximum membership degree. Though this method leads to better performance as compared to the controller without tuning, it has some limitations reflected by the dependence on initial rule base, and the difficulty in defining the desired output of the fuzzy controller as it is related to entire input space (Gürocak and Lazaro 1994).

In order to mitigate the problem that some system variables can vary during transitional period, functions based on the absolute value of the normalized system variable were applied to adjust rule weights. Karasakal *et al* (2011) suggested a tuning method using the absolute values of the normalized system parameters, i.e., system error in this study, as the weight values. With the normalized system error, a self-tuning rule weight was specified. The performance of the proposed self-tuning method was demonstrated to be efficient on both linear and non-linear systems (Karasakal *et al* 2011).

An index was proposed by Gacto *et al* (2010) in order to facilitate the tuning of fuzzy logic controller. The index maintained the interpretability of fuzzy rule base while enhancing the accuracy of the membership functions. The proposed index was composed of three metrics. Arule-selection module was added to the tuning mechanism based on database to reduce the complexity of the proposed model. The tuning mechanism modifies the parameters and shape of membership functions. A post-processing algorithm, i.e., a multi-objective evolutionary algorithm, was also developed to ensure accuracy of linguistic interpretation and efficiency of the controller. The results concluded that their objectives were achieved via the proposed technique (Gacto *et al* 2010).

With the increasing number of input variables to the fuzzy logic systems, the fuzzy rule base becomes more complicated which may jeopardize the robustness of the system and require more computing resources. In view of this, a fuzzy rule-based classification model for high-dimensional controllers was proposed by Alcala-Fdez *et al* (2011). This method involved three stages including fuzzy association rule extraction for classification, candidate rule prescreening, and genetic rule selection and lateral tuning (Alcala-Fdez *et al* 2011). From the experimental results, it was concluded that the proposed method for solving the high-dimensional problems had reduced computational burden without impeding performance.

2.2 Review of Bearing Fault Detection

Machine bearings are failure-prone due to the heavy load and harsh working conditions, particularly in wind turbines which are often operated under unpredictable and volatile wind conditions. Bearing failure could also cause breakdown of the entire system, and hence increased downtime and maintenance cost. Therefore, they are the major focus of condition monitoring. To detect the incipient bearing faults (bearing faults at an early stage), a solution is developing an online condition monitoring system (Sugumaran and Ramachandra 2011).

A rolling element bearing consists of inner and outer races, a cage, as well as rolling elements. Defects, such as crack, can occur in any of these components and will result in high frequency vibrations. Moreover, the severity of the wear can change the vibration pattern. In most cases, it is possible to identify the component of the bearing that is defective based on specific vibration frequencies, called fault characteristic frequencies (Girdhar and Scheffe 2004).

2.2.1 Sensors for bearing fault detection

Bearing fault detection methods have been extensively studied. Methods based on

time-domain analysis, frequency-domain or time-frequency domain analyses of acquired signals have been developed. According to Marichal *et al* (2011), sensing methods used for bearing fault detection methods can be divided into four groups: vibration measurement, acoustic measurement, temperature measurement, and wear-debris analysis. Of the four, vibration measurement and acoustic measurement are most widely used and are discussed in detail in this section.

1. Vibration Sensors

Piezoelectric accelerometers are popular for vibration signal collection due to their low cost, easy to use and excellent performance in the frequency bands of interest. Considering the fault excited resonance, bearing faults can often be more easily detected in the resonance frequency band as the signal-to-noise ratio (SNR) is higher in this frequency band as compared with other frequency regions (McFadden and Smith1984).

2. Acoustic Sensors

Well-known acoustic sensors include air-coupled ultrasound transducer, piezoelectric ultrasound transducer, etc. According to the comparison study by Rezaei *et al* (2011), certain acoustic features were responsive to variation in operational condition and to machine damage.

The performance of fault detection methods previously developed varies with the size and location of the fault as well as the method applied.

2.2.2 Vibration measurement and fault detection

Vibration monitoring has been used as an effective way of bearing fault detection and diagnosis (Hajnayeb *et al* 2008). Vibration measurement can be used as a source of information for fault detection and monitoring, as the noise or vibration signals that are obtained from machines often convey information about the occurrence and

locations of faults (Choi and Kim 2007).

As mentioned above, the defects of bearings can occur on the roller, the inner race or the outer race. When the defect contacts the mating component, a vibration sensor can detect mechanical impulses. Such impulses usually repeat periodically (Liang and Bozchalooi 2010).

Therefore, many fault detection techniques are based on the analysis of the vibration signals. However, the vibration signal measured from a mechanical system contains both fault information and back ground noise, as well as interference signal components caused by gear meshing, shaft misalignment, etc (Liang and Bozchalooi 2010). Hence, a series of methods aiming at distinguishing the fault information from the raw vibration signals and eliminating the effect of back ground noises have been developed. In general, the majority of bearing fault detection methods is based on the analysis of signals in time-domain, frequency domain, or time-frequency domain, though other methods are also reported.

2.2.3 Bearing fault detection methods

Fault detection of bearings based on vibration measurement has been developed to a great extent. Usually, the processing method composes of pre-processing of the data, analysis of the processed data and diagnosis of the bearing condition according to certain criteria. In the pre-processing stage, some features of the raw vibration data are usually extracted to facilitate subsequent processing such as filtering the noise and amplifying part of the signal of interest. To analyze the processed vibration data, one or a combination of several techniques are employed. Detailed methods are introduced in this section.

2.2.3.1 Time domain methods

In a review study by Tandon and Choudhury (1999), bearing detection methods based

on vibration methods and acoustic methods are examined. They pointed out that the commonly used time domain parameters included peak value, root-mean-square (RMS), probability density, kurtosis and skewness (Tandon and Choudhury 1999).

1. Time-domain parameters

The processing results obtained from the root-mean-square of vibration signal alone were somewhat unsatisfactory (Tandon and Choudhury 1999). As such, other time-domain parameters including probability density, kurtosis, and skewness were used for fault detection as well. The probability density of acceleration signal of a healthy bearing obeys Gaussian distribution, while a faulty bearing leads to a non-Gaussian distribution due to peaks in the vibration signal resulted from defect impact.

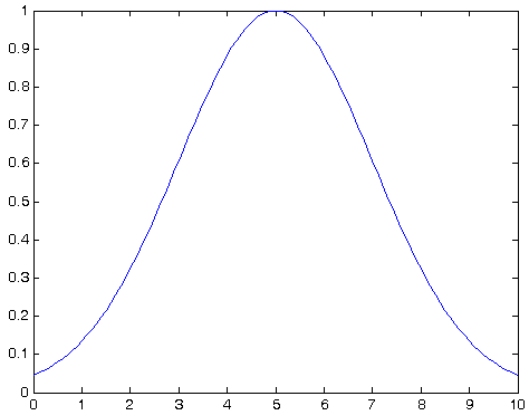

Figure 2.1. Gaussian distribution with mean value 5 and variance 2

The implementation of kurtosis value on bearing fault detection was proposed by Dyer and Stewart (Tandon and Choudhury 1999). Kurtosis values calculated from raw vibration signals for bearing defect detection provides a guideline to distinguish the healthy bearings and faulty bearings. For healthy bearings, the acceleration signal obeys Gaussian distribution and the kurtosis value is around 3. When fault occurs on bearings, the kurtosis values of the acceleration signals increase in most cases (Tandon and Choudhury 1999). Though the kurtosis value can be above 3 for a healthy bearing and drop to around 3 for a faulty bearing due to many other factors, kurtosis value is still a good indicator as it has a reference value, i.e., 3, which does

not change with bearing size, type, load, speed, etc and hence will be adopted in the fuzzy control and monitoring platform proposed in this study.

Another parameter, peak-to-peak value, is defined as the difference between the maximum peak and minimum peak, which reflects the strength of the raw vibration signal. Calculation results in this thesis have shown that peak-to-peak value increases under most conditions when defects occur on bearings, regardless of the type and location of the defect. Therefore, it can also be used as a reliable bearing fault indicator, together with kurtosis, for more accurate detection decisions.

In addition, shock value of the vibration signal can also indicate the defects of bearings, but the shock value could be inappropriately estimated by direct demodulation in the shock pulse method (SPM) (Li, He, *et al* 2008).Therefore, a method, which is based on improved redundant lifting scheme (IRLS), is proposed by Li, Meng, *et al* (2008) to make the evaluation of bearing condition more accurate. The severity of outer race bearing fault can be detected with this method while its performance under other conditions are not demonstrated.

2. Adaptive noise cancellation methods

Adaptive noise cancellation (ANC) methods are developed in order to reduce noise mingled with raw vibration signals. This method is based on exploring the reference noise signals from the same source as signals containing fault information(Park *et al* 2002).This approach has been widely applied, including in medical field (Gagne *et al* 2010), hydro geophysics magnetic field (Dalgaard *et al* 2012), fault detection (McFadden and Smith 1984), etc. It has also been successfully implemented to reduce background noise in speech signals, adaptive antenna arrays, and vibration signals from many sources such as rotating machines, rolling element bearings, etc., for monitoring and detection purposes (Chaturved and Thomas 1981).

In a sense, noise cancellation is an optimized filtering method. The raw signal containing fault information is filtered by subtracting the reference noise from it.

Therefore, the noise can be reduced or eliminated (Widrow *et al* 1975). This method is useful if the mask noise is strong and regular techniques are not capable of extracting the target information from raw vibration data. However, the ANC technique may result in higher cost in computation due to the optimization process. Also, to provide a reference vibration signal, more sensors will be mounted on the machines. For mechanical system like wind turbines, it may not be desirable or feasible to have many sensors built in the limited space.

2.2.3.2. Frequency domain methods

A number of methods such as fast Fourier transform, high-frequency resonance methods, and spectral kurtosis methods have been applied to bearing fault detection (Rai and Mohanty 2007, Antoni2006, Wang and Liang 2011). Root-mean-square is also applied to frequency domain analysis.

1. Fast Fourier Transform (FFT)

Though FFT can detect faults when SNR is sufficiently high, it is generally not used alone for bearing fault detection because it is ineffective in handling noisy data and is blind to time-varying events (Rai and Mohanty 2007). Therefore, it was often used as part of other frequency-domain or time-frequency domain methods.

For example, to strengthen the performance of feature extraction, a signal pre-processing method, i.e., amplitude recovery method combined with fast Fourier transform(Liu *et al* 2010), was developed. This pre-processing method can distinguish the fundamental frequency of the system so that the amplitudes of other frequencies will be available for further spectrum analysis.

2. Bandpass filtering methods and shock pulse methods

Bandpass filtering methods have been implemented in both time and frequency domains. In frequency domain applications, the theoretical basis is that structural resonances appear in high frequency bands. Therefore, defects such as spalling of

bearing races or rolling elements can be recognized by a sensor fixed at the resonance frequency (Tandon and Choudhury 1999).

3. High frequency resonance methods

The high frequency resonance (HFR) technique is proposed based on the idea that the contact between the bearing fault and its mating surface excites resonance, i.e., high frequency "ringing" which damps out quickly before the next contact. This high frequency resonance is amplitude modulated at the fault characteristic frequency. Therefore, the fault can be detected by amplitude demodulation. The HFR method contains two main steps, i.e., bandpass filter the raw signal and then amplitude demodulate the bandpass filtered signal. The bandpass filter is designed corresponding to the resonant frequency in order to eliminate unwanted vibration signals. The pre-processed signals are demodulated by envelope detectors, where carrier frequencies and resonant frequencies are eliminated (Tandon and Choudhury 1999). The main difficulty in the HFR method is the proper selection of the center frequency and bandwidth of the bandpass filter as the resonance frequency band is unknown beforehand.

4. Spectral kurtosis method

This method is generally based on short-time Fourier transform (STFT). Based on the STFT result at each time window, the frequency range of interest is divided into a number of frequency windows (narrow band filters). Then the raw signal is filtered by these filters. Then a kurtosis value is calculated for the data obtained by each filter. A certain process such as window merging (Wang and Liang 2011) is then applied to these kurtosis values. The merged window with the highest kurtosis value will serve as the bandpass filter to process the raw signal. The processed signal is then amplitude demodulated to detect the envelope and hence the fault characteristic frequency. Related studies have also been reported in (Antoni 2006, 2007, Antoni and Randall 2006). The main problems with this method include the large amount of computations

required to obtain the spectral kurtosis values and the difficulty in distinguishing noise and fault impulses for signals with strong noise.

2.2.3.3 Joint time-frequency methods

The time-frequency domain analysis in the context of fault detection can provide information related to not only whether a fault exists but also when it exists. Several types of time-frequency methods have been developed which include wavelet transform,

1. Wavelet transform methods

Wavelet transform decomposes a signal into different frequency ranges (scales), and then analyze each of them with a resolution matching its scale. Wavelet based transform is widely used in tool condition monitoring (Zhu *et al* 2009), bearing fault detection (Singh *et al* 2009, Kankar *et al* 2011a, Kankar *et al* 2011b, Sheen 2009, Li, Meng *et al* 2008, Hou *et al* 2010), as well as structural health monitoring (Taha *et al* 2006), etc.

In fault detection, discrete wavelet transform is usually employed because it provides fast signal decomposition and guarantees both energy conservation and exact signal reconstruction (Watson and Addison 2002). Along this line, a wavelet-transform based method was introduced for fault detection of rolling element bearings by Li, Meng, *et al* (2008) to facilitate the fault recognition. The discrete wavelet transform is also applied particularly for diagnosis of ball bearing race faults (Prabhakar *et al* 2002).A harmonic wavelet-transform based method was proposed to extract the characteristics of faulty rolling bearing (Hou *et al* 2010). Continuous wavelet transform was also used in bearing fault detections (Kankar *et al* 2011b) with reasonable performance. The main difficulty with the wavelet transform methods is that they require the selection of a proper wavelet basis function as well as the related parameters such as the scale and shape factor.

2. Wigner-Ville Distribution methods

Wigner-Ville distribution (WVD) is a Fourier transform of a signal's instantaneous covariance function. The WVD method has been applied to detect gear and bearing failures in transmission systems (Choy *et al* 2009) and to diagnose conditions of rotating machinery (Wang and Chen 2011).

The WVD method is demonstrated to be effective in identifying bearing defects. The severity of the defects can be reflected by the intensity in WVD. However, it cannot independently indicate the type and location of defects and thus combination with the time and frequency analysis is required to satisfy further indication requirement (Choy *et al* 2009).

The advantages and limitations of WVD are also proved by Wang and Chen (2011). The study concludes that under the bearing fault detection case, the WVD method is of the highest diagnosis sensitivity among investigated time frequency domain methods, i.e., short-time Fourier transform (STFT), wavelet analysis (WA), and the Wigner-Ville distribution (WVD). However, it suffers from cross-term interference for multi-component signals. In addition, when frequency variations are nonlinear, the WVD cannot present a localized distribution.

2.2.3.3 Fuzzy related methods

Working conditions of bearings can be reflected by extracted characteristics from vibration measurement signals. Most of the methods based on frequency-domain analysis require human interpretation to assess bearing conditions according to the analysis results. Therefore, many automated diagnosis methods based on fuzzy logic and neural network are proposed. These fuzzy-related techniques help to decide the working conditions of bearings with less human intervention. Machine learning methods have demonstrated to be applicable and useful with vibration measurement (Sugumaran and Ramachandra 2011).

Study based on artificial intelligence was also developed with wavelet-transform

based feature extraction method. The wavelet-transform based method relies on minimum Shannon entropy criterion. Several wavelets with different bases have been examined. To extract statistical characteristics, complex Morlet wavelet is adopted with minimum Shannon Entropy Criterion (Kankar *et al* 2011a). With the pre-processed signals as inputs to an artificial intelligence structure, the category of bearing faults could be classified (Kankar *et al* 2011a).

2.3 Limitations of Previous Studies and Motivation of Proposed Study

The main limitation of the previous studies is the separation of the control and monitoring tasks though the two share much of the devices and information. This obviously leads to the duplicated development effort and investment. More importantly, the separation of the two closely related tasks also makes the control actions less relevant without taking the actual machine condition into account.

As such, this thesis is directed towards the development of a platform that will facilitate the integration of the control and monitoring tasks. The on-line information can be easily shared without using additional devices and the control will be more responsive not only to the working conditions (e.g., wind speed) but also to actual machine conditions (e.g., healthy or faulty). To facilitate remote applications, a wireless module will also be developed. It should be pointed out that the proposed platform is not intended to be a final system. Instead, it provides a stage for proof of concepts. More sophisticated control and monitoring algorithms can be incorporated into it in future.

As for the control part, though conventional control methods such as PID control can perform many tasks, they require accurate mathematical models which may be difficult to develop for non-linear systems. Fuzzy logic methods allow people to transfer linguistic rules into models. Prior experience can be embedded into the controller directly without complex modeling, which simplifies the design and improves the efficiency. For this reason, the fuzzy control approach will be adopted in

this thesis.

To make the controller more adaptive to system and process changes, a tuning mechanism will also be developed. However, considering the rapid changes in the system and process in the context of wind turbine control, a tuning mechanism should be computationally efficient. Therefore, a tuning mechanism directly modifies the rule base weight is preferred, as the change in the shape of membership functions does not significantly influence the control of the gearbox speed. For this reason, a self-tuning mechanism based on the input variables will be developed in this study

For monitoring, kurtosis and peak-to-peak values will be used because of their advantages as reviewed above. In addition, these two indicators require much less human intervention as compared with many other methods. They can be easily and quickly computed from the vibration signals for on-line applications. Furthermore, they are much less expertise-demanding which is important for fast field implementation.

Chapter 3. Design of the Bearing Monitoring and Gearboxes Speed Control System

As mentioned before, the main purpose of this study is to control the motor (generator in a real wind turbine) speed in response to the bearing conditions. Considering the volatile and unpredictable wind turbine working conditions, a fuzzy control approach is adopted because of its tolerance for imprecision of the data, uncertainty of the process, and partial truth of the prior knowledge, as well as its ability to model non-linear functions of arbitrary complexity and to make use of the experience of domain experts. In addition, it is easy to implement and versatile.

In the design of shaft speed controller, speed change $C(i)$ and speed error $E(i)$ are selected as the inputs. Triangular membership is used due to its less time-consuming feature while preserving a satisfying performance. Center of maximum is employed as defuzzification method because it provides a reasonable output.

For the bearing fault monitoring part, kurtosis values and peak-to-peak values are used as fault indicators and as inputs to the fuzzy logic controller. The kurtosis value and peak-to-peak value are treated as separate inputs to the fuzzy logic controller. These two parameters are then combined with the speed change and speed error as the inputs to the integrated shaft speed controller. Detailed explanation of this method is presented in the following sections of this chapter.

3.1 Structure of Fuzzy Logic Controller

The fuzzy logic controller shown in Figure 3.1 consists of three main modules, i.e., a fuzzification module, a fuzzy inference engine (membership functions and rule base), and a defuzzification module. Input variables will be fuzzified before entering the fuzzy inference engine, and the output is determined according to the membership functions and rules. Then the output is defuzzified into crisp values.

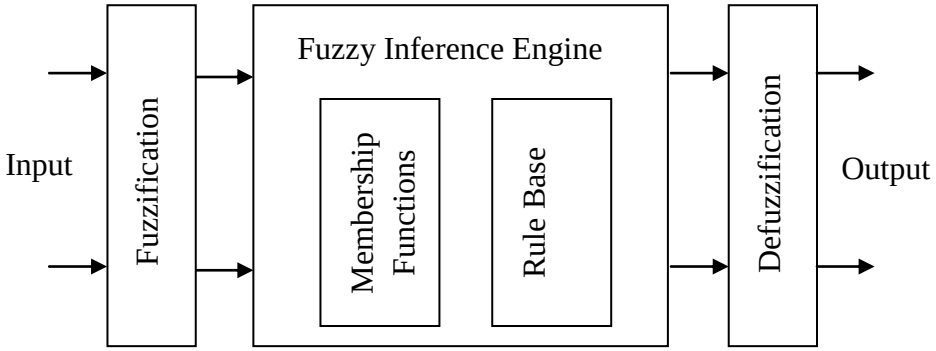

Figure 3.1. General structure of a fuzzy logic controller

3.2 Inputs and Output of the Fuzzy Logic Controller

In this system, there are four inputs to the fuzzy controller. To control the rotating speed of the shaft, speed error $E(i)$ and shaft speed change $C(i)$ are selected as the inputs. As mentioned previously, the fault indicators, kurtosis and peak-to-peak values are the other two inputs to the fuzzy logic controller. The structure of the proposed controller is illustrated in Figure 3.2, where ω_{ref} is the reference rotational speed specified by the user, and ω is the real rotational speed. Detailed explanation to the parameters shown in Figure 3.2 is stated in the following subsections.

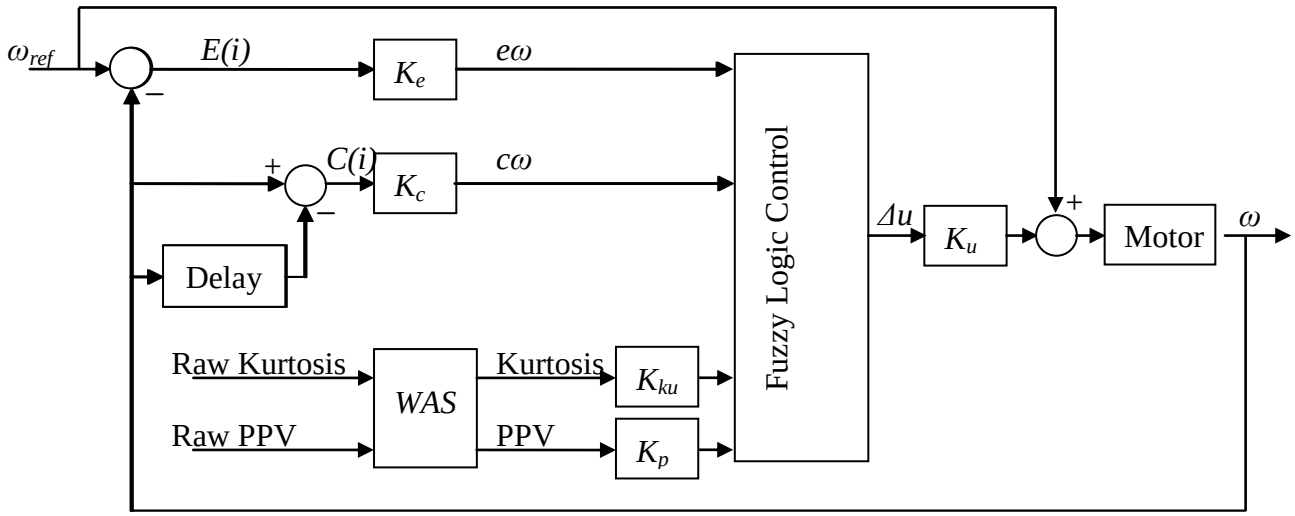

Figure 3.2. Developed fuzzy logic control system

1. Error and Change of Error

The rotating speed given by a user is set as the reference speed ω_{ref}. The actual speed of the shaft ω is obtained from an encoder mounted on the shaft. For any ω measured in a sampling period i, the error of speed and the change of the speed are defined as follows:

$$E(i)=\omega_{ref} - \omega(i) \tag{3.1}$$

$$C(i) =\omega(i) -\omega(i - 1) \tag{3.2}$$

where $E(i)$ and $C(i)$ stand for speed error and speed change, respectively.

2. Kurtosis

Kurtosis value represents a statistical feature of vibration signals. The kurtosis value of a distribution is defined as:

$$\text{Kurtosis} = \frac{\xi(x-\mu)^4}{\sigma^4} \tag{3.3}$$

where μ is the mean of x, σ is the standard deviation of x, and $\xi(t)$ represents the expected value of the quantity t.

Kurtosis is a measure of impulsiveness of a signal. As the majority of bearing faults (this thesis focuses on only bearing faults) lead to impulse trains in the vibration signals, kurtosis has proven to be an effective bearing fault indicator (Wang and Liang 2012, Wang and Liang2011, Antoni and Randall 2006, Combet and Gelman 2009, and Antoni2007).

Kurtosis is also a criterion of how outlier-prone a distribution is. The kurtosis of the normal distribution is 3. Distributions that are more outlier-prone than the normal distribution have kurtosis greater than 3; distributions that are less outlier-prone have kurtosis less than 3(Matlab 2012ahelp for statistics box). Hence, the kurtosis value can be used to distinguish the Gaussian background noise (kurtosis = 3), discrete vibration (similar to sinusoids with kurtosis values close to 1.5), and the fault induced

impulses with kurtosis values much higher than 3.In this chapter, kurtosis is abbreviated as Kur.

3. Peak-to-peak value

Peak-to-peak value (PPV) is the difference between the maximum and minimum values in an input or a sequence of inputs (Matlab 2012a help for DSP system toolbox). It is also a measure of the strength of the vibration signal from system and is useful to distinguish the fault severity level.

4. Change of voltage

The output of the fuzzy logic system is the change of output voltage to modify the rotating speed of the shaft. The shaft speed is controlled by an analog voltage value, and therefore, the output of the controller is designed as the change of output voltage to avoid transfer between voltage value and corresponding shaft speed value.

3.3 Input and Output Variables and Scaling Factors

1. Scaling factors for Speed Error and Speed Change

The scaling factor of each input variable is designed according to corresponding requirements.

The scaled speed error $e\omega$and scaled speed change $c\omega$ are obtained by multiplying speed error $E(i)$and speed change $C(i)$ by their corresponding scaling factors. Speed error $e\omega$ is given by Equation (3.4), as the range of speed error should be from $-\omega_{ref}$ (at the moment of stop), i.e., $E_{min}(i) = 0 - \omega_{ref}$, to maximum value of input reference speed ω_{ref} (at the moment of start)i.e., $E_{max}(i) = \omega_{ref} - 0$:

$$e\omega = E(i) * K_e \tag{3.4}$$

where K_e is the scaling factor. To map the speed error into the universe of discourse, i.e., [-1, 1], the scaling factor can be expressed as $K_e = 1/\omega_{ref}$.

Similarly, speed change $c\omega$ is given by Equation (3.5).

$$c\omega = E(i) * K_c \tag{3.5}$$

where K_c is the scaling factor. The minimum speed change is $-\omega_{ref}$(at the moment of stop), i.e., $E_{min}(i) = 0 - \omega_{ref}$, and the maximum speed change is ω_{ref} (at the moment of start), i.e., $E_{max}(i) = \omega_{ref} - 0$. Therefore, K_c can be obtained by $K_c = 1/\omega_{ref}$.

2. Scaling function for kurtosis value

The kurtosis value range is decided based on the calculation results of experimental data obtained in our lab at the University of Ottawa and from literature (the Case Western Reserve University Bearing Data Center)as well as simulation data in order to account extreme situations.

Based on the results, the range of kurtosis values is specified from 0 to 50. All potential input kurtosis values that may exceed this range will be treated as 50, and same mechanism applies to the input peak-to-peak values. Table 3.1 in Appendix I shows the kurtosis values computed for various cases based on the data from the Case West Reserve University.

As it is shown in Table 3.1 (refer to Appendix I), the kurtosis values of the healthy bearings range from 2.765 to 2.956 which, as expected, are very close to that of the Gaussian noise. For faulty bearings, the kurtosis varies from 5.318to 23.542, except the cases of the outer race fault with a fault size of 0.014" in diameter, for which the kurtosis values are lower than expected (between 2.941 and 3.797).

Based on the experimental data obtained from our lab at the University of Ottawa (Table 3.2 in Appendix I), the kurtosis values of healthy bearings are from 3.241 to 5.426 and those of faulty bearings vary from 6.146 to 44.200. The relatively high kurtosis for file B06H could be caused by the gear interference. Though the ranges of

kurtosis values for healthy and faulty bearings fall into different ranges with different experimental setups, it is observed that the kurtosis values of healthy bearings are mostly around 3 and those of the faulty bearings are above 3 except for a few outlier cases. Therefore, kurtosis can be used as a fault indicator.

It is also observed in Table 3.1 (refer to Appendix I) that the peak-to-peak values of healthy bearings are between 0.590 and 0.690 which are much lower than those of the faulty bearings (between 0.800 and 13.300). In addition, the peak-to-peak value tends to increase with fault size (again, except the 0.014" fault) but is insensitive to the changes in horsepower (load) and shaft rotational speed. Therefore, peak-to-peak value can avoid the influence introduced by load and shaft speed when diagnosing the condition of a bearing.

From the experimental result of data from the University of Ottawa in Table 3.2 (Appendix I), the peak-to-peak values of healthy bearings are from 0.161 to 0.310 and those of faulty bearings are from 0.491 to 1.763, except for the B18 and B19 data. From the results of B01 to B08, the peak-to-peak values of healthy bearings are much lower than those of faulty ones no matter how the load changes.

The B18 and B19 data are from the fan end senor with two faulty bearings installed at both ends. The peak-to-peak values for these two data sets are not within the PPV range of faulty bearings discussed above. This may result from the different sensor locations, and the two faulty bearings could counteract the vibration effects. As within the same test condition, the peak-to-peak value is able to indicate the difference between healthy and faulty bearings.

Therefore, the peak-to-peak value can be used as an indicator of fault existence as well as fault severity.

The distributions of kurtosis and peak-to-peak values based on the Case Western Reserve University data are plotted in Figure 3.3(a) and 3.3(b), respectively.

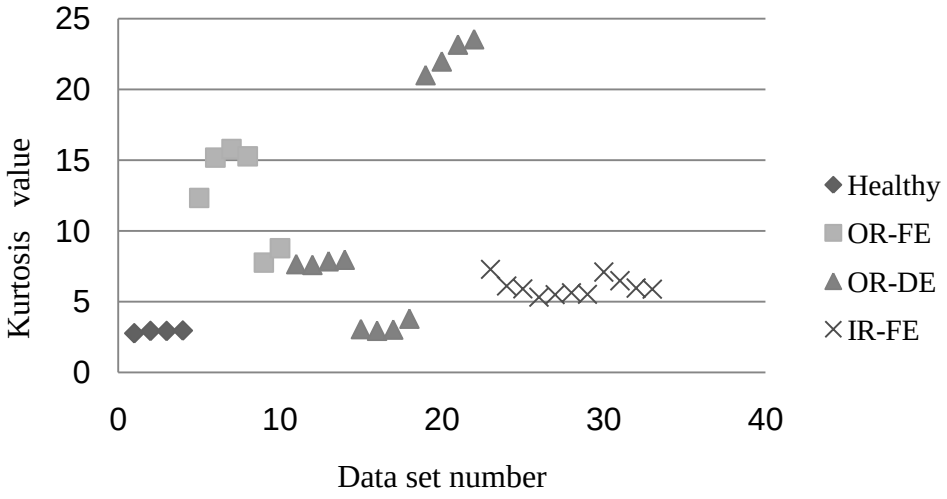

(a) Distribution of kurtosis values from literature

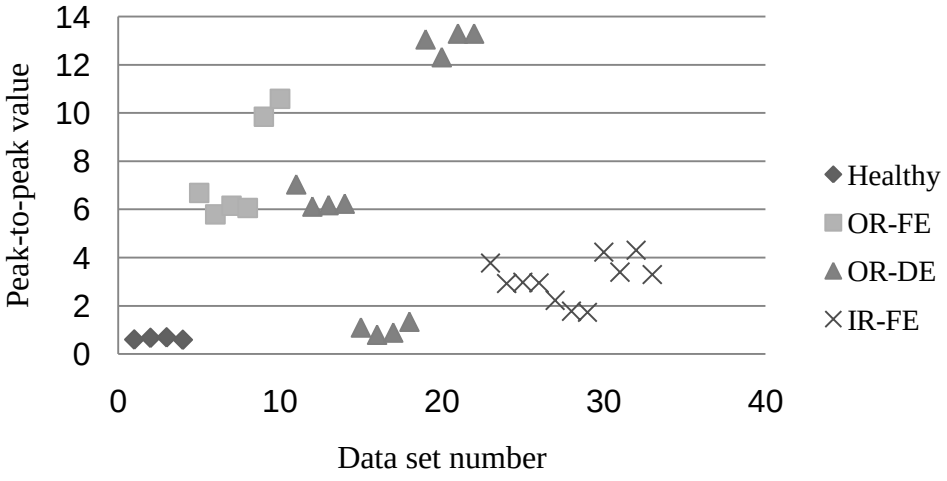

(b) Distribution of peak-to-peak values

Figure 3.3. (a) Distribution of kurtosis values, and (b) Distribution of peak-to-peak values

In addition, the kurtosis values of simulated signals have been calculated to examine some extreme conditions with very strong impulsiveness and low background noise that may occur but difficult to create experimentally. This will help to ensure that the

range of kurtosis is wide enough to cover most of the bearing conditions. The signal $x(t)$is composed of simulated signal $s(t)$ and Gaussian noise $n(t)$, i.e.,

$$x(t) = s(t) + n(t) \tag{3.6}$$

The simulation signal $s(t)$ in describes the vibrations of a faulty bearing with fault characteristic frequency of $1/T_p$ (Liang and Bozchalooi2010):

$$s(t) = \sum_{m=-M}^{M} L_m e^{-\beta(t-mT_p-\sum_{i=-m}^{m}\tau_i)} \cos\left(\omega_r(t-mT_p-\sum_{i=-M}^{m}\tau_i)\right)u(t-mT_p-\sum_{i=-M}^{m}\tau_i) \tag{3.7}$$

where M is half of the number of the fault generated impulses, L_m is the amplitude of mth fault impulse, $\beta$the decay parameter, T_p is the time period corresponding to the fault characteristic frequency, τ_i presents the effect of random slippage of the rollers and is modeled as a uniformly distributed random variable with a zero mean and a standard deviation of $0.01T_p$, ω_r is the excited resonance frequency, and $u(t)$ is a unit step function. Comparing with the original model in the previous study (Liang *et al* 2000), the signal model defined by Equation (3.7) has a minor modification in phase shift of the cosine function that does not affect the simulation result.

The sampling frequency is set to 20 kHz, and all the other parameters in Equation (3.7) are listed in Table 3.3. The fault character frequency is accordingly $1/T_p$=125 Hz.

Table 3.1. Parameters used in equation (3.7)

Parameter	M	L_m	β	T (ms)	ω_r (rad/s)
Value	250	1	1500	8	$2\pi \times 2$k

The simulation results with two different signal-to-noise ratios (SNRs) are presented

in Figure 3.4 and the corresponding kurtosis values are 17.553 and 19.116, respectively.

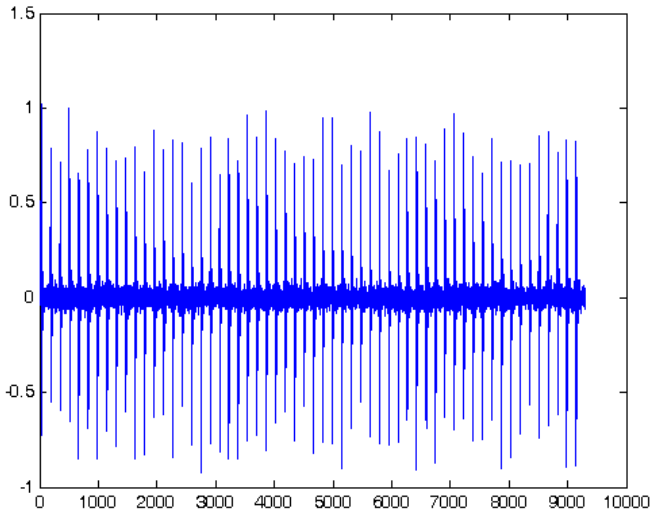

(a) SNR = 30, Kurtosis = 17.553

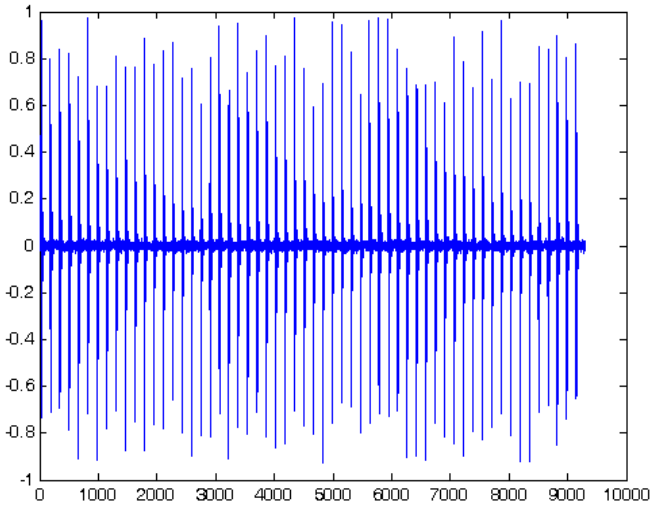

(b)SNR = 40,Kurtosis = 19.116

Figure 3.4. Simulation data with (a) SNR =30, and (b)SNR =40

To reduce computing time, it is desirable to map crisp kurtosis values to fuzzy domain based on resolution needs. The kurtosis values around 3 are most ambiguous which could be the result of either a healthy bearing or a bearing with an incipient fault. Hence this kurtosis range deserves closest scrutiny and requires the highest resolution. On the other hand, any kurtosis value between 30 and 50 would indicate a high

possibility of a bearing fault. It is hence unnecessary to further divide this range (30 to 50) into more sub-ranges which means more fuzzy sets and more computational requirement. Similarly, a kurtosis below 2.7 is unlikely to be caused by a transient impulsive fault signal and thus there is no need to further divide kurtosis values below 2.7.

As such, the kurtosis values from 0 to 50 are divided into 9 intervals and its corresponding intervals on the universe of discourse is listed next to them as shown in Table 3.4. This table is for calculating the scale factors for input kurtosis. Here the kurtosis value 3 corresponds to the zero point of universe of discourse. As reasoned above, higher resolution is required for kurtosis values closer to 3, whereas the resolution is reduced with the increase of the kurtosis (when it is above 3). From Table 3.4, the largest interval [30,50] is specified because within this interval the occurrence of fault or other accidents can be assured. For kurtosis interval [0, 3] that corresponds to [-1, 0], the values are evenly distributed.

The mapping functions for each interval can be calculated according to Table 3.4. As each pair distributes linearly within its interval, when mapping a value from the left column, i.e., x_r, to corresponding fuzzified value, i.e., x_f, the mapping function can be expressed as:

$$x_f = K_{ku} * (x_f - x_{rmin}) + x_{fmin} \tag{3.8}$$

where $K_{ku} = \frac{x_{fmax} - x_{fmin}}{x_{rmax} - x_{rmin}}$.

The mapping functions for each pair can be calculated by Equation (3.8).

After applying the tuning mechanism with vibration data from lab at the University of Ottawa to the results shown in Table 3.4, the first node is modified from 3.5 to 5.426 with k = 1.5, which provides a more reasonable result when this membership functions is designed for the experimental setup at the lab in the University of Ottawa.

Table 3.2. Mapping of kurtosis values of data from literature (from the Case Western Reserve University Bearing Data Center)

Intervals of kurtosis values $[x_{rmin}, x_{rmax}]$	Intervals of fuzzified kurtosis values $[x_{fmin}, x_{fmax}]$
[0.00,3.00]	[-1.00,0.00]
(3.00,3.50]	(0.00,0.25]
(3.50,7.00]	(0.25, 0.50]
(7.00,28.00]	(0.50, 0.75]
(28.00,50.00]	(0.75, 1.00]

3. Mapping function for peak-to-peak value

The peak-to-peak values of the data from literature and lab at the University of Ottawa are shown in the third column of Tables 3.1 and Table 3.2 (refer to Appendix I), respectively. The peak-to-peak values of healthy bearing data from literature are around 0.6 to 0.69 and the peak-to-peak values of faulty bearing data from the same resource ranges from 0.8 to 13.06 with only few of the results dropped under 1.0.

The calculation of PPV based on experimental data from University of Ottawa also demonstrates that under the same experimental set-up, the peak-to-peak values of healthy bearings(from 0.161 to 0.310) are much lower than those of faulty bearings (from 0.491 to 1.763).Similar to the mapping principle of kurtosis values, lower peak-to-peak values require higher resolutions as a slight change in PPV of lower range may result in a different bearing condition. The peak-to-peak mapping ranges based on vibration signal from literature(Case Western Reserve University) are listed in Table 3.5.

The mapping function of PPV of each interval pair, can be calculated based on Table

3.5. When mapping a value from the left column, i.e., x_y, to corresponding fuzzified value, i.e., y_f, the mapping function can be expressed as:

$$y_f = K_p * (y_f - y_{rmin}) + y_{fmin} \quad (3.9)$$

where $K_p = \frac{y_{fmax} - y_{fmin}}{y_{rmax} - y_{rmin}}$.

The mapping functions for each pair can be separately calculated by Equation (3.9).

Table 3.3. Mapping result of peak-to-peak values

Intervals of PPV $[x_{rmin}, x_{rmax}]$	Intervals of fuzzified PPV $[x_{fmin}, x_{fmax}]$
[0.000, 1.400]	[0.000, 0.330]
(1.400, 4.000]	(0.330, 0.670]
(4.000, 12.000]	(0.670, 1.000]

With experimental results from our lab at the University of Ottawa, which is shown in Table3.2 in Appendix I, the tuning result based the mapping result in Table 3.5 is adjusted. The mapping result with available data in Table 3.2 in Appendix I, with k = 2, is shown in Table 3.6. The results mapped the experimental results into fuzzy domain reasonably well.

Table 3.4.Mapping results of peak-to-peak values

Intervals of PPV	Intervals of fuzzified PPV
[0.000, 0.510]	[0.000, 0.330]
(0.510, 4.000]	(0.330, 0.670]
(4.000, 12.000]	(0.670, 1.000]

4. Output voltage adjustment

The amount of output voltage adjustment *cu* is obtained by multiplying scaled change

of voltage $\Delta u$by its scaling factor K_u, which is decided by maximum output voltage u_{max}, i.e.,

$$cu = \Delta u * K_u \tag{3.10}$$

where

$K_u = 1/u_{max}$, when Δu belongs to NL to PX (to be explained later)

$K_u = u_{max}$, when Δu belongs to NX (to be explained later)

The above output scaling factor is defined so as to cause minimal disturbance to the system while it is running normally and to generate a sufficient negative offset to slow down or shut down the system, depending on severity, in the presence of fault.

3.4 Membership Functions

The universes of discourse of input speed error, speed change and kurtosis value, as well as output voltage change are in the range of [-1, 1]. The universe of discourse of the input peak-to-peak value is in the range of [0, 1] as PPV is always positive and zero is the ideal but unachievable condition. The fuzzy sets used in this control system are referred to as NX, negative extra large; NL, negative large; NM, negative medium; NS, negative small; ZERO, zero; PS, positive small; PM, positive medium; PL, positive large, and PX, positive extra large, respectively. Please note that some of the membership functions only use part of these fuzzy sets.

To simplify computation, the triangular membership functions are used for all inputs and outputs. However the numbers of fuzzy sets are different as detailed below.

The membership functions for speed error and speed change both cover seven fuzzy sets from NL to PL, which are shown in Figure 3.5(a) and Figure 3.5(b). The fuzzy sets from left to right are, NL, NM, NS, ZERO, PS, PM, and PL, respectively.

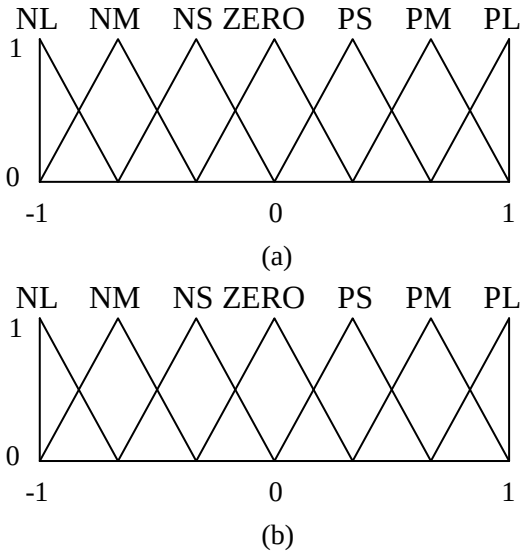

Figure 3.5.Membership functions for input:(a) speed error, and(b) speed change

The membership function for input kurtosis value and output voltage change include nine fuzzy sets from NX to PX, respectively, which are shown in Figure 3.6. According to the mapping result in Table 3.4, in the interval [-1,0], the mapping factor is constant. Hence, the four fuzzy sets are evenly distributed. For symmetric purpose, four fuzzy sets were placed in the negative axis. The fuzzy sets from left to right are NX, NL, NM, NS, ZERO, PS, PM, PL and PX, respectively.

The membership function for input peak-to-peak value covers four fuzzy sets and is demonstrated in Figure 3.7. According to the mapping result listed in Table 3.5,interval [0,1]is divided into 3 sections, which corresponds to the four fuzzy sets shown in Figure 3.7.The fuzzy sets from left to right are ZERO, PS, PM and PL, respectively.

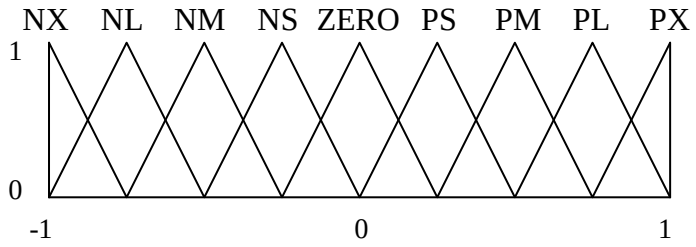

(a)Membership functions for input kurtosis

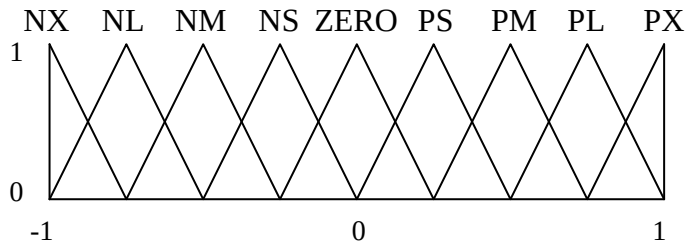

(b)Membership functions for output voltage change

Figure 3.6. Membership functions for (a) input kurtosis, and (b) output voltage change

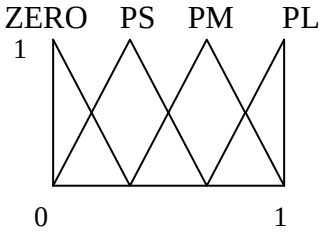

Figure 3.7. Membership functions for input peak-to-peak value

3.5 Rule Bases

As discussed above, there are four inputs to the fuzzy logic engine. Each combination of speed change, speed error, kurtosis value and peak-to-peak value is related to a control action. The control action is triggered by the associated rule(s). The rule(s) are determined based on developer's knowledge and experience, or experimental results. For example, if speed change and speed error are positive small while kurtosis value and peak-to-peak value are zero, the output voltage change is negative small to compensate for the output voltage. The description of each rule is in the format

illustrated as follows:

If $e\omega$ is PS, $c\omega$ is PS, kurtosis value is ZERO and peak-to-peak value is ZERO Thencu is NS.

As the four inputs will lead to a large number of combinations (i.e., rules) if they are considered simultaneously in a single rule base, it is extremely time-consuming and error-prone to develop a rule base in such a way. Therefore, two rule bases are developed separately, one for the speed error and speed change, and the other for kurtosis and PPV. The rules related to speed error and speed change are shown in Table 3.7. In this case, the output voltage change only involves two inputs, i.e.,$e\omega$ and $c\omega$.

Table 3.5. Rules related to speed error and speed change inputs

$e\omega$ / Δu / $c\omega$	NL	NM	NS	ZERO	PS	PM	PL
NL	PL	PL	PL	PM	PM	PS	ZERO
NM	PL	PL	PM	PM	PS	ZERO	NS
NS	PL	PM	PS	PS	ZERO	NS	NM
ZERO	PM	PM	PS	ZERO	NS	NM	PM
PS	PM	PS	ZERO	NS	NS	NM	NL
PM	PS	ZERO	NS	NM	NM	NL	NL
PL	ZERO	NS	NM	PM	NL	NL	NL

For the rule base related to kurtosis value and peak-to-peak value, the rules are first categorized into three groups, i.e., general rule 1, general rule 2 and general rule 3, with different possibility of fault occurrence, i.e., healthy, probably faulty or faulty.

Table 3.8 shows the rule bases under these three categories, where H, L, F represent healthy, probably faulty or faulty, respectively, and A represents accidental impact.

General rule 1: Fault is considered to occur if:

kurtosis falls into PM, PL or PX, and PPV falls into PS, or

kurtosis falls into PM, PL or PX, and PPV falls into PM or PL, or

kurtosis falls into PS and PPV falls into PM or PL

General rule 2: Faultis considered likely to occur ifkurtosis and PPV both fall into PS areas.

General rule 3: No fault is to occur ifkurtosis and PPV both fall into ZERO areaor one of them falls into ZERO area and the other one falls into PS area.

Table 3.6. Rules for fault occurrence judgment based on kurtosis and PPV

Kur / PPV	ZERO	PS	PM	PL	PX
ZERO	H	H	A	A	A
PS	H	L	F	F	F
PM	A	F	F	F	F
PL	A	F	F	F	F

In addition, if kurtosis is PM, PL or PX and PPV is ZERO, or kurtosis is ZERO and PPV is PM or PL, it is considered as a random event (e.g., accidental knock by a person walking by). To strengthen the last rule, a wait-and-see (WAS) logic module is placed before the inputs of kurtosis and PPV. The purpose of the wait-and-see logic is to filter accidental high value of kurtosis value or peak-to-peak value. Only when the condition (kurtosis is PM, PL or PX and PPV is ZERO, or kurtosis is ZERO and PPV

is PM or PL) lasts a long period, this condition should be considered as fault occurrence.

3.5.1 Wait-and-see logic

The principle of this wait-and-see logic is to filter out accidental high values in input kurtosis values and peak-to-peak values. The kurtosis and peak-to-peak values are processed similarly and, therefore, only the procedure for kurtosis is described in detail.

Kurtosis value is calculated based on a certain number of sample points, which can be customized as needed. For example, if we set the sample points as 10,000, we can obtain one kurtosis value for every 10,000 sample points.

To simplify discussion, we call this kurtosis value as raw kurtosis value, which is the input of the WAS logic. The WAS module first reads in j raw kurtosis values. Then it will map these values into the nine groups corresponding to fuzzy sets, i.e., NX, NL, NM,NS, ZERO, PS,PM, PL, and PX. Next it calculates the size of each group and find the group that occupies most of input raw kurtosis values. The group of the maximum size is noted as Group_max. At last, it will output the maximum value or mean value of the Group_max.

By this process, this logic can filter out the unreasonably high or small outlier values within a period of time. The time period can be set when the number of input raw kurtosis is assigned. For example, if j is 10, the waiting time is $10 \times T_{kur}$, and if j is 30, the waiting time is longer, i.e., $30 \times T_{kur}$, where T_{kur} is the time spent for calculating one raw kurtosis value. The amount of the raw kurtosis input values can be customized as needed. Using this WAS logic as the pre-processing of the kurtosis values before they enter the fuzzy logic controller can avoid taking accidentally changed kurtosis values as input to the fuzzy controller.

Similar process is applied to peak-to-peak values before it is fed into the fuzzy logic system. The WAS logic reads in a certain number of raw peak-to-peak values and maps them into four groups as there are four fuzzy sets for PPV inputs. Then the group containing the maximum numbers will be distinguished and the maximum value or mean value of this group will be output. The wait-and-see logic is summarized in the following flowchart (Figure 3.8).

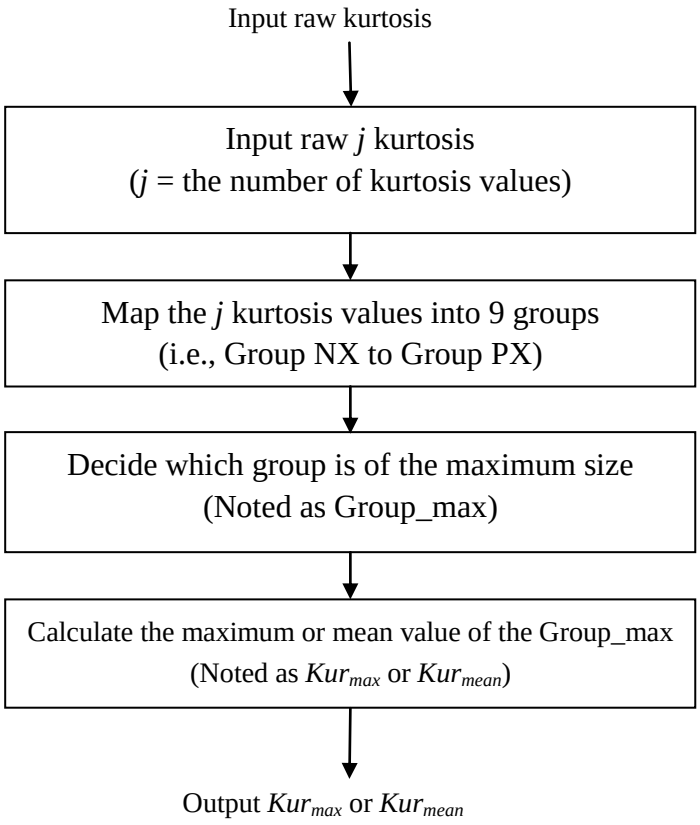

Figure 3.8. Flowchart of wait-and-see logic

After implementing the wait-and-see logic to the fuzzy logic system, the fuzzy inference engine will calculate the corresponding output according to the rule base. When there is no fault detected, i.e., general rule 3, the fuzzy logic controller obeys the rules from Table 3.7 so that it maintains the output at the level set by the user. When the bearing fault is to occur or likely to occur as described by general rules 1

and 2, the output voltage change falls into NX fuzzy set. Then the shaft will be slowed down or stopped.

3.6 Fuzzy Inference and Defuzzification

With the fuzzy inference process illustrated in Figure 3.10, the fuzzy membership degree is calculated based on the Mamdani-type implication(Driankov *et al* 1996). In this study, maximum-minimum fuzzy inference method is used. In each rule, the membership degree of output Δu is determined by the minimum of membership degrees of all its inputs. To illustrate, consider rule 1 for example. The implication can be carried out using Equation (3.11) , where $\mu_{PM-1}(\Delta u)$ represent the membership degree of output Δu, its subscript PM-1 indicates that the related fuzzy set is PM and the number of the rules is 1, $\mu_{NS}(c\omega)$ denotes the membership degree of the NS fuzzy set of input $c\omega$, and the same format applies to other variables, i.e., $\mu_{NM}(c\omega)$, $\mu_{ZERO}(kurtosis)$, and $\mu_{ZERO}(PPV)$.

$$\mu_{PM-1}(\Delta u) = \min[\mu_{NS}(c\omega), \mu_{NM}(c\omega), \mu_{ZERO}(kurtosis), \mu_{ZERO}(PPV)] \quad (3.11)$$

The membership degrees of the output for other rules are specified in the same way. After calculating the membership degree of output of each rule, the membership degree of a fuzzy set in output domain is determined by the maximum value of membership degree of outputs of all contributing rules, as it is shown in Equation (3.12).

$$\mu_{PM}(\Delta u) = \max[\mu_{PM-i}(\Delta u) | i \in \Phi] \quad (3.12)$$

where Φ is set of rules that are triggered by the inputs and hence will contribute to the $\mu_{PM}(\Delta u)$ fuzzy set.

Through Figure 3.10 to Figure 3.13, the contributing outputs include PM, PL and NX fuzzy sets. Therefore, the $\mu_{PL}(\Delta u)$ and$\mu_{NX}(\Delta u)$are decided in the same way as described above. $\mu_{PL}(\Delta u)$, $\mu_{NX}(\Delta u)$ and $\mu_{PM}(\Delta u)$ will then be used to calculate

the crisp output with Equation (3.13).

In this thesis, the center of maximum (COM) defuzzification method is used as it is readily available in the LabView toolbox. With this fuzzification method, the fuzzy logic controller first identifies the scaled membership function with the greatest degree of membership. The fuzzy logic controller then determines the typical numerical value for that membership function. The typical numerical value is the mean of the numerical values corresponding to the degree of membership at which the membership function was scaled. The COM defuzzification method (LabView PID and Fuzzy Logic Toolkit User Manual) is illustrated in Figure 3.13 with the following equation:

$$u = \frac{\sum_{p=1}^{P} \mu_p C_p}{\sum_{p=1}^{P} \mu_p} \tag{3.13}$$

where p is the number of relevant rules, u is the crisp output, C_p represents mean value for maximum membership function and μ_p is the degree of membership among relevant membership functions.

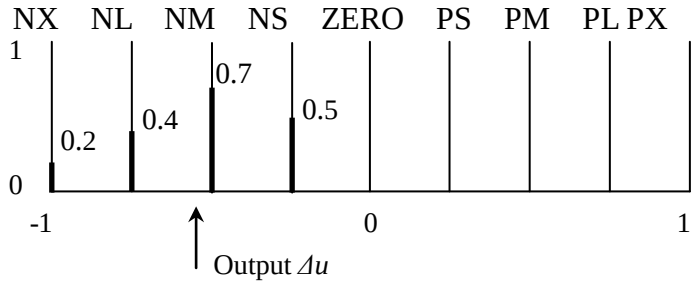

Figure 3.9. Demonstration of COM defuzzification method

With the data shown in Figure 3.9, the calculation result based on the COM defuzzification method is as follows:

$$u = \frac{0.20 \times (-1) + 0.4 \times (-0.75) + 0.70 \times (-0.50) + 0.50 \times (-0.25)}{0.20 + 0.40 + 0.70 + 0.50} = -0.54$$

Each value of a single input may be related to one fuzzy set or two fuzzy sets. Therefore, four inputs can trigger at most16 (=2 ×2 ×2 ×2)rules.

The COM reference process is further illustrated with the following 16 rules:

1. If speed change is NS, speed error is NS, kurtosis is ZERO and PPV is ZERO, then output voltage change is PS.
2. If speed change is NS, speed error is NS, kurtosis is ZERO and PPV is PS, then output voltage change is PS.
3. If speed change is NS, speed error is NS, kurtosis is PS and PPV is ZERO, then output voltage change is PS.
4. If speed change is NS, speed error is NS, kurtosis is PS and PPV is PS, then output voltage change is NX.
5. If speed change is NS, speed error is NM, kurtosis is ZERO and PPV is ZERO, then output voltage change is PM.
6. If speed change is NS, speed error is NM, kurtosis is ZERO and PPV is PS, then output voltage change is PM.
7. If speed change is NS, speed error is NM, kurtosis is PS and PPV is ZERO, then output voltage change is PM.
8. If speed change is NS, speed error is NM, kurtosis is PS and PPV is PS, then output voltage change is NX.
9. If speed change is NM, speed error is NS, kurtosis is ZERO and PPV is ZERO, then output voltage change is PM.
10. If speed change is NM, speed error is NS, kurtosis is ZERO and PPV is PS, then output voltage change is PM.
11. If speed change is NM, speed error is NS, kurtosis is PS and PPV is ZERO, then output voltage change is PM.
12. If speed change is NM, speed error is NS, kurtosis is PS and PPV is PS, then output voltage change is NX.
13. If speed change is NM, speed error is NM, kurtosis is ZERO and PPV is ZERO, then output voltage change is PL.
14. If speed change is NM, speed error is NM, kurtosis is ZERO and PPV is PS, then output voltage change is PL.

15. If speed change is NM, speed error is NM, kurtosis is PS and PPV is ZERO, then output voltage change is PL.
16. If speed change is NM, speed error is NM, kurtosis is PS and PPV is PS, then output voltage change is NX.

The mechanism of how the 16 rules work is demonstrated in Figure 3.11 to Figure 3.14, which are listed in Appendix II. Each row illustrates a relevant rule with the four inputs, i.e., input speed change, input speed error, input kurtosis value, and input peak-to-peak value, as well as the output voltage change, arranged from left to right respectively. In each rule, the input value corresponds to a membership degree. The minimum membership degree of the four inputs decides the membership degree of the output. The figure is drawn in Figures 3.11 to 3.14 which can be referred to in Appendix II, in the order of the rules from 1 to 16 listed above.

As discussed above, in the fuzzy implication procedure, consequent implication of each method is decided by the minimum membership degree of its inputs. The combined output is composed of the outputs of all the triggered rules and their corresponding membership degrees, which is shown in Figure 3.10.As the crisp output voltage change is calculated based on the mean value of the maxima of each contributive fuzzy set. The crisp output value is pointed out by the arrow in Figure 3.10 and it is calculated with Equation (3.13).

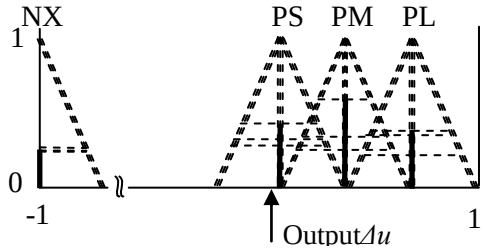

Figure 3.10. Combined output of the fuzzy inference system

This value will then be multiplied by a scaling factor K_u before combining with the set value ω_{ref}. Finally, the combined result, i.e., $\omega_{ref}+K_u \times \Delta u$, will be delivered to execution devices to control the system.

3.7 Self-tuning Mechanism

Since the ranges of kurtosis values of healthy bearing vibration signals and faulty bearing vibration signals may extend or shift to a certain degree under different experimental conditions, a self-tuning mechanism is introduced to modify the scaling factor of kurtosis values in response to such changes. For the same reason, the scaling factor of peak-to-peak value also requires adjustment when applied for different working conditions, such as different shaft dimensions, different bearing types, etc.

This mechanism enables the fuzzy controller to tune the scaling factors to provide better performance in fault diagnosis. As shown in Table 3.1 and Table 3.2 in Appendix I, though the range of peak-to-peak values of healthy bearings are approximately in a fixed range, the results based on the data from the literature (i.e., from 0.590 and 0.690) are quite different from that of the lab at the University of Ottawa (i.e., from 0.161 to 0.310). Similarly, the range of PPV of faulty bearings from literature (i.e., 0.800 and 13.300) does not cover the range of PPV of healthy bearings from the University of Ottawa (i.e., 0.491 to 1.763). Therefore, a tuning technique is desirable to identify the boundary between PPV of healthy bearings and that of faulty bearings. When considering the kurtosis values, the same situations occur.

The adjustment of scaling factors for the input kurtosis value and PPV can enhance the adaptability of the controller on different platforms.

In this study, the tuning is done based on the idea that a gap exists between kurtosis values (or peak-to-peak values) of healthy and faulty bearings. To evaluate the gap properly, the mean value of kurtosis values (or peak-to-peak values) of healthy bearings and the amount of deviation from this value should be considered.

The membership function is originally established according to pre-required knowledge. For input kurtosis, the original fuzzy sets are determined by evaluating the distribution of a group of values including both healthy and faulty conditions. As this is decided by limited number of kurtosis values, the fuzzy set needs further adjustment through its operation. This principle also applies to input peak-to-peak value.

The tuning mechanism is explained based on input peak-to-peak value. For input kurtosis values, the tuning mechanism is similar and hence we present only the tuning mechanism for the input peak-to-peak value as follows.

We denote the nth input peak-to-peak value as $PPV(n)$. The mean value of peak-to-peak values prior to the nth input peak-to-peak value is calculated, which is expressed as $PPV_{mean}(n)$. The difference between the nth input peak-to-peak value and the mean value of previous peak-to-peak values can be expressed as:

$$\Delta(n) = PPV(n) - PPV_{mean}(n) \tag{3.14}$$

Similarly, for the $(n+1)$th input peak-to-peak value, it is written as:

$$\Delta(n+1) = PPV(n+1) - PPV_{mean}(n+1) \tag{3.15}$$

After the calculation above, the ratio of $\frac{\Delta(n+1)}{\Delta(n)}$ is calculated. Then the decision is made based on the following two cases (Note: $|x|$ denotes the absolute value of x):

Case 1: If $|\frac{\Delta(n+1)}{\Delta(n)}| > k$ (where k is the coefficient for weighting the gap between PPV of healthy bearings and that of faulty bearings), $PPV(n+1)$ will replace the first node in fuzzy set, i.e., node_1 shown in Figure 3.15. In this case, k is set to 1.5. The sensitivity of the controller increases with a smaller value of k while the controller shall be less sensitive if a greater k is selected.

Under this case, after replacing the original node_1 with the $PPV(n+1)$, PPV_{mean} will remain at its current value for the next calculation, i.e., $\Delta(n+2) = PPV(n+2) - PPV_{mean}(n+1)$.

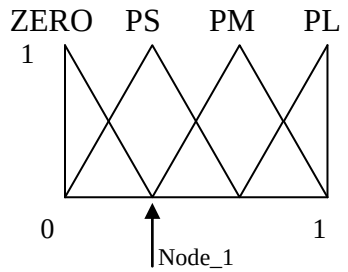

Figure 3.15.Node_1 of peak-to-peak value fuzzy set

Case 2: if $|\frac{\Delta(n+1)}{\Delta(n)}| < k$, the difference between the nth input peak-to-peak value and the mean value of previous peak-to-peak values is calculated by:

$$\Delta(n+1) = PPV(n+1) - PPV_{mean}(n+1) \quad (3.16)$$

Node_1 will be replaced by adding $\Delta(n+1)$ to Node_1, i.e.,

$$\text{Node\_1}+\Delta(i+1) \rightarrow \text{Node\_1}$$

The mapping results of kurtosis value and peak-to-peak values of data from the University of Ottawa are discussed in section 3.3. In this way, only a small number of inputs is required to determine the preliminary mapping of membership functions. It is able to adjust the mapping factor during the operation and makes the proposed technique to be more adaptive to different working conditions.

Chapter 4. Experimental Setup and Results

4.1 Wired System Setup

The experimental setup for testing the algorithm is introduced in this section. The program developed using Labview software is tested on a wired platform shown in Figure 4.1 whose structure is summarized in Figure 4.2.

The devices used for the system are listed as follows:

- Hitachi Inverter (Model: SJ 200 -022NFU2)
- Marathon electronic motor (Model: AVJ 56T34F5306J P)
- Accu-CODER encoder (Part No.: 755-B-H-1024-R-HV-D-P/10.00-A-N-N)
- Placid Industries magnetic particle CLUTCH PHC-50
- IMI High frequency industrial ICP accelerometer 623C01
- National Instrument multifunction DAQ USB-6212 BNC
- Intel Core 2 PC with Windows XP OS

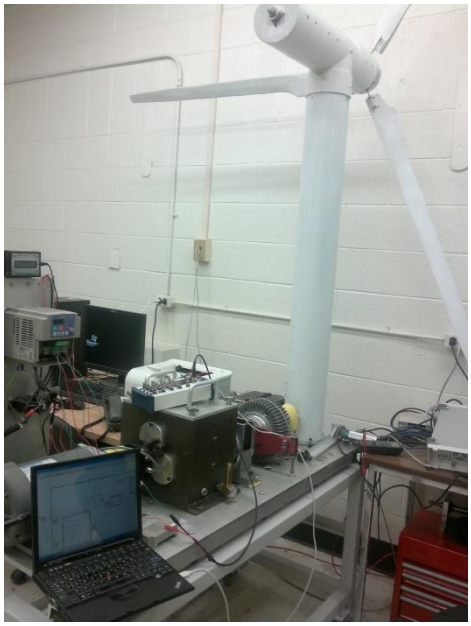

Figure 4.1. Experimental setup at the University of Ottawa Lab

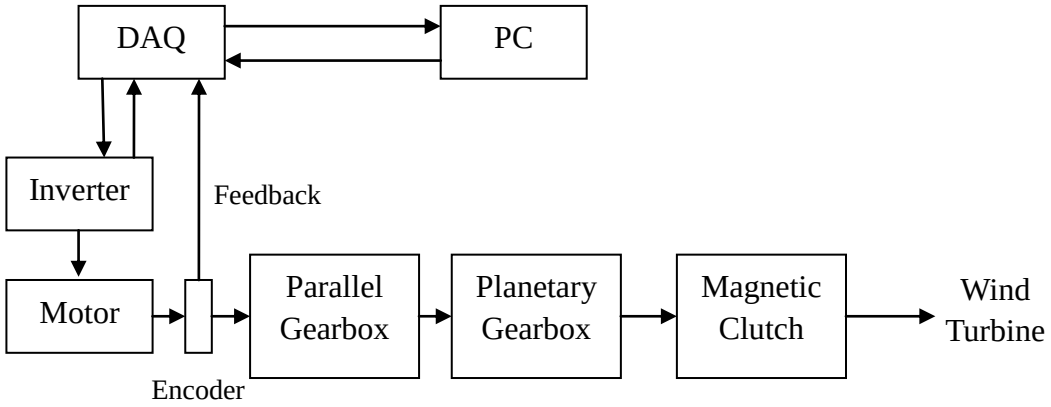

Figure 4.2. Structure of wired system

All major devices are shown in Figure 4.2. The wind turbine system consists of a parallel gearbox, a planetary gearbox, a magnetic clutch and a wind turbine rotor with three blades. Between the wind turbine rotor and the gearboxes, a magnetic clutch with output from 0 to 30lbs·ft is placed to imitate the possible loads in real wind turbine implementation. Modifying the current supplied to the magnetic clutch will change its output torque. A calibrated curve showing the relationship between the input current and output torque is provided by the supplier (Placid Industries, Incorporation) of the wind turbine test rig.

A 2.24 kW 3600 rpm AC motor is used to drive the shaft connected to the gearboxes. An inverter from Hitachi is connected to control the speed and switch of the motor. This inverter is programmable and accepts external control. An analog output port and a digital port on the DAQ are connected to the external control board of the inverter in order to control the output voltage and switch to the motor., which control the speed and switch of the motor, respectively. To obtain the feedback signal, a line drive encoder with resolution of 1024 per revolution is mounted on the output shaft of the motor. The output of the encoder is connected to the digital input on the DAQ to read in the frequency of the shaft. This DAQ collects data acquired from the encoder and delivers the commands to all other devices. It is able to communicate with PC via USB port so that it can work on a laptop outside.

The data fed into the control system for monitoring is vibration signals acquired by accelerometer sensors. There are eight differential BNC analog inputs with16-bitresolution when the sampling rate is at 400k samples per second per channel. This satisfies data acquisition rate of vibration data (12k samples per second).

4.2 Wireless System Diagram

Wind turbines are usually installed in fields far away from the control center, and therefore, a remote communication device is preferred. Also, wireless platform avoids complex cable system required for signal transfer. Long distance communication is able to be done via several platforms. The purpose of the wireless platform is to test that the developed algorithm in this study can be implemented wirelessly. In this study, we used a pair of wireless modules mainly for experimental purpose, which is shown in Figure 4.3. This experimental system can be easily transferred into other wireless communication platform according to the need in the future.

4.2.1 Wireless system structure

The wireless system is composed of two wireless modules as well as the devices introduced in section 4.1. The structure of the wireless set-up is similar to the wired one.

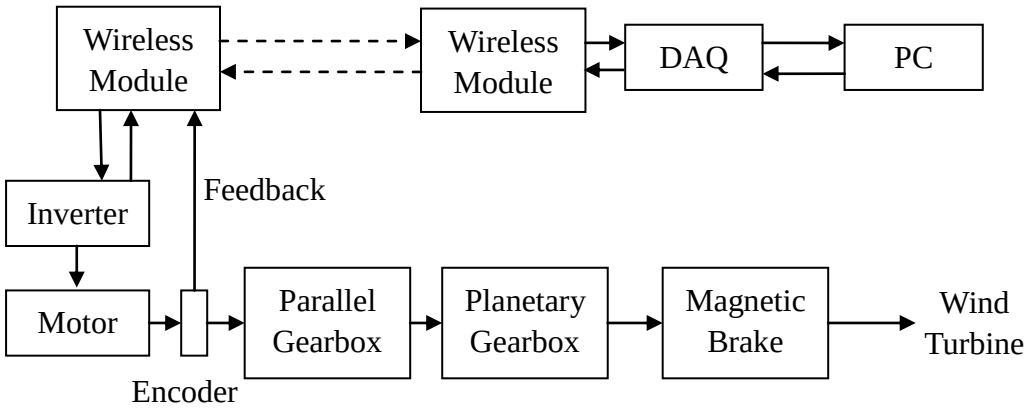

Figure 4.3. Structure of wireless communication platform

4.2.2 Wireless Module

This wireless kit has two terminals, which are the master and the slave respectively. The specifications of the two terminals are respectively listed in Tables 4.1 and 4.2.

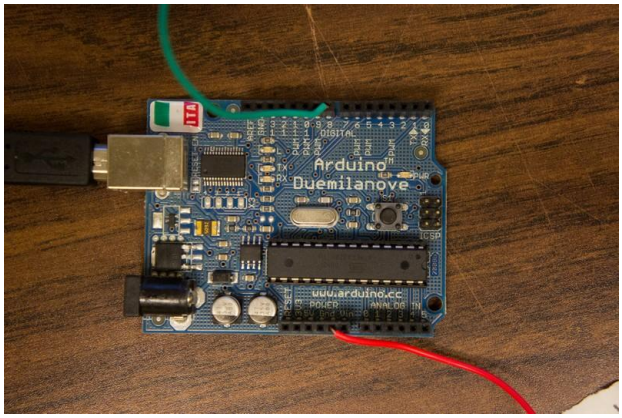

(a) Arduino Duemilanove board with an ATMega328 microcontroller

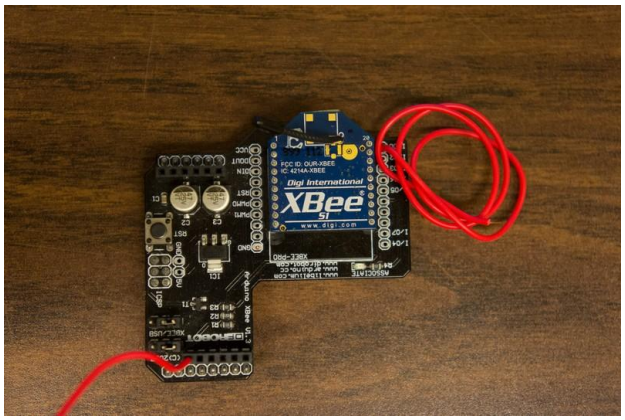

(b) Xbee S1 wireless module

Figure 4.4. Components of wireless terminals

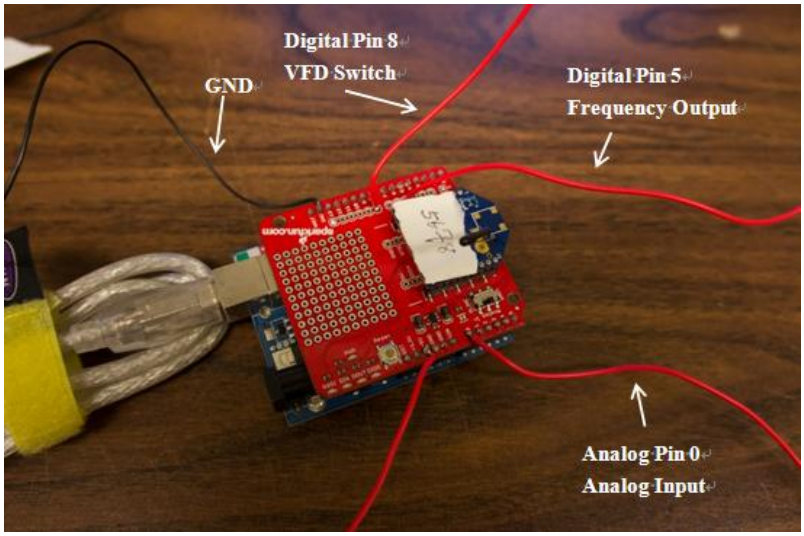

Figure 4.5. Master terminal

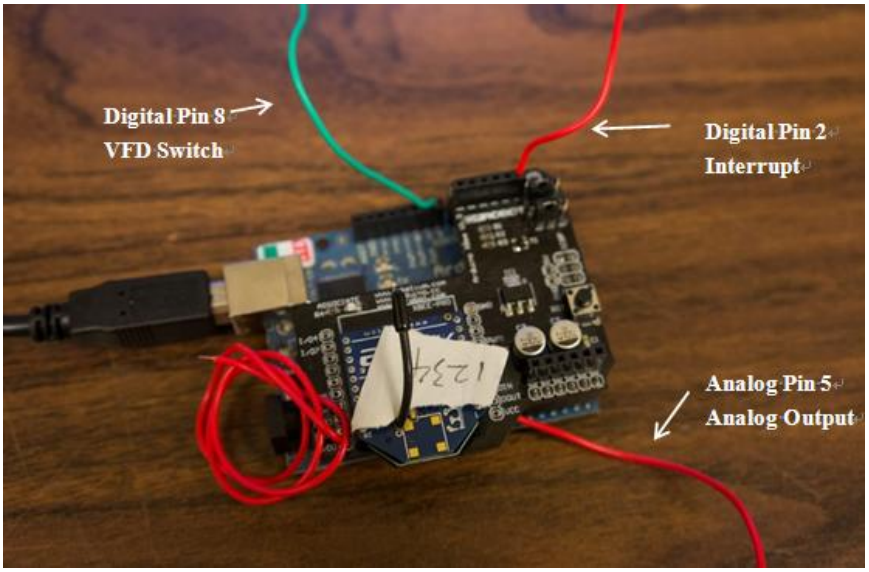

Figure 4.6. Slave terminal

Table 4.1.Specifications of the master terminal

Master terminal	
Input	0-5v analog input; TTL digital input
Output	Frequency output (0-20KHz)
Working frequency	2.4GHz
Data transfer rate	250Kbps
Power supply	DC power (7V to 12V)

Table 4.2. Specifications of slave terminal

Slave terminal	
Input	0-5v analog input
Output	Frequency output (0-20KHz)
Working frequency	2.4GHz
Data transfer rate	250Kbps
Power supply	DC power(7V to 12V)

Each terminal consists of one Arduino Duemilanove board with an ATMega328 microcontroller and an Xbee S1 wireless module, which are respectively shown in Figure 4.4 (a) and Figure 4.4(b). The master (Figure 4.5) is connected to DAQ and the slave (Figure 4.6) is wired to inverter and encoder. Both digital and analog signals can be transmitted between the two terminals wirelessly. The slave terminal is defined to produce analog signal (0V to 5V) and digital signal, and the master is to receive digital signal from DAQ and to transmit commands to the slave terminal.

4.2.3 Programming for the wireless modules

The algorithm is written in Arduino software (Version 1.0.1). This developing environment can compile codes in C programming language and upload the compiled codes to the Arduino board. The flowchart of the program is shown in Figure 4.7.The master terminal generates the command enabling the slave to output an analog signal (0V to 5V) and digital signal to inverter. The slave terminal reads in impulses from encoder to calculate its frequency and transmits the frequency value to the master terminal. Then the master generates a square waveform at the corresponding frequency. All the transmission is completed in a wireless manner.

The transmission between the two terminals is introduced in this paragraph. The master terminal reads in an analog value from DAQ via the A/D converter of the

master terminal. This analog value of 10-bit is then mapped into an 8-bit value to facilitate the transmission. The eighth analog pin (abbreviated as “pin8” in the subsequent paragraphs) on the master terminal serves as the switch to control the ON/OFF of the inverter. If pin8 is at a high voltage, it prints out “H”, otherwise an “L” is printed out. Before the data is sent out, an “S” identifies the beginning of the data. When the slave terminal detects this character, it starts to receive the data from the master terminal, where the data consists of “S” indicating the beginning, eight-bit data, and “H” or “L” as status indicator.

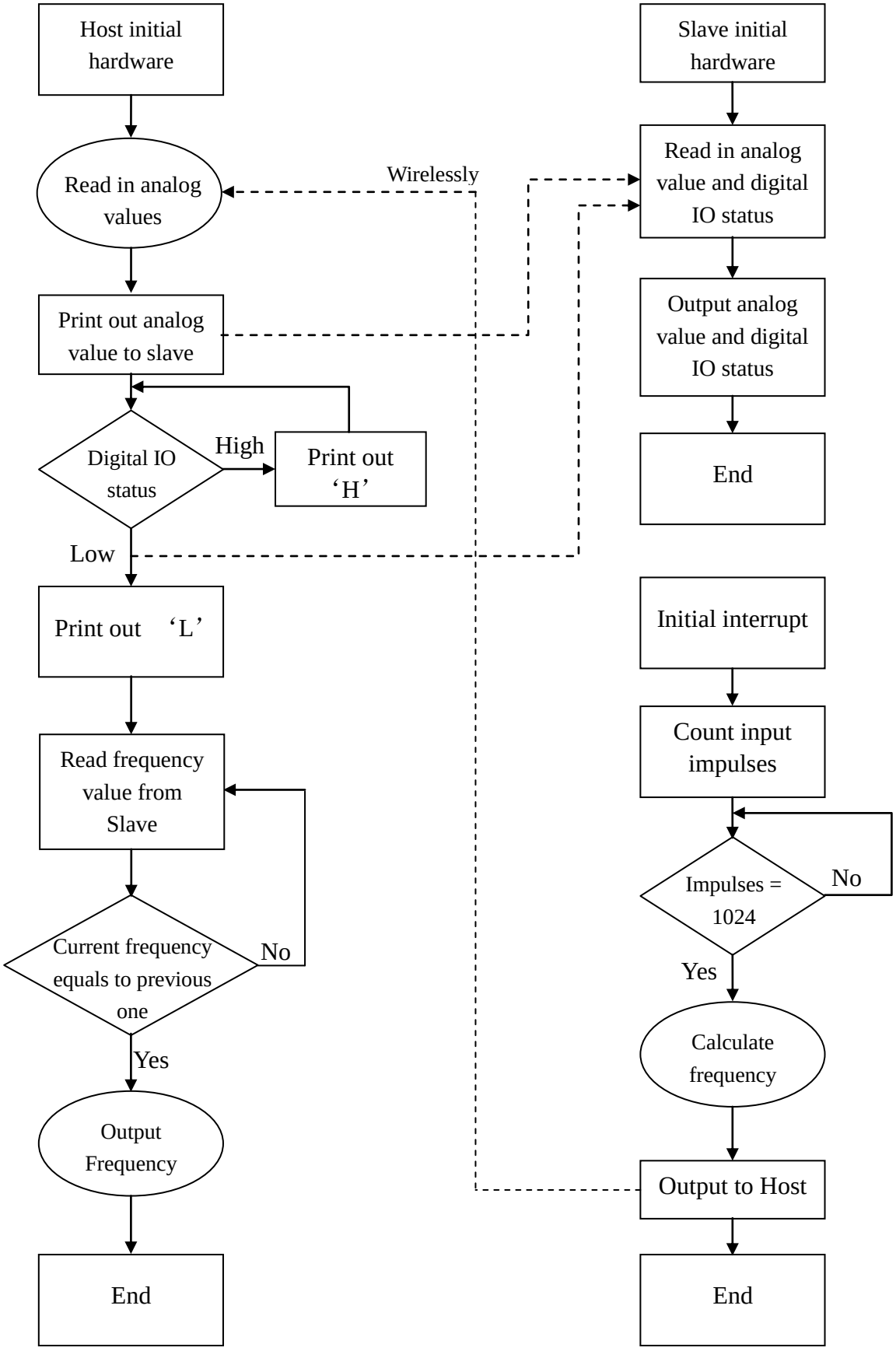

Figure 4.7. Flowchart of the program developed for wireless modules

To calculate the frequency, the interrupt is used on the slave terminal. When the counter counts 1024 impulses, the frequency of the input impulses will be calculated by dividing the number by the time accumulated during counting. The slave then transmits this value via serial port to the master terminal, and the master terminal generates a square waveform of the same frequency at digital pin 5, which then feeds the waveform into the DAQ.

4.3 Experimental Results

Experiment based on the wireless platform was carried out and the corresponding performance is examined in this section. The results of experiments performed under several different conditions are introduced in the following subsections.

4.3.1 Speed control with healthy bearings

4.3.1.1 Experimental result of varying speeds at constant load

In this situation, the load added by the magnetic clutch was fixed to 10 lbs ft. The shaft speed was set to 300 RPM, 270 RPM and 180 RPM at three stages, respectively. The result is illustrated in Figure 4.8. As shown in this figure, the overall tolerance band was maintained within 1.18% with an overshoot of 3.95%. The step response time was 0.06 s. The green line represents the user-desired shaft speed value, whereas the blue line is the real shaft speed value. The same legend applies to figures hereafter in this chapter.

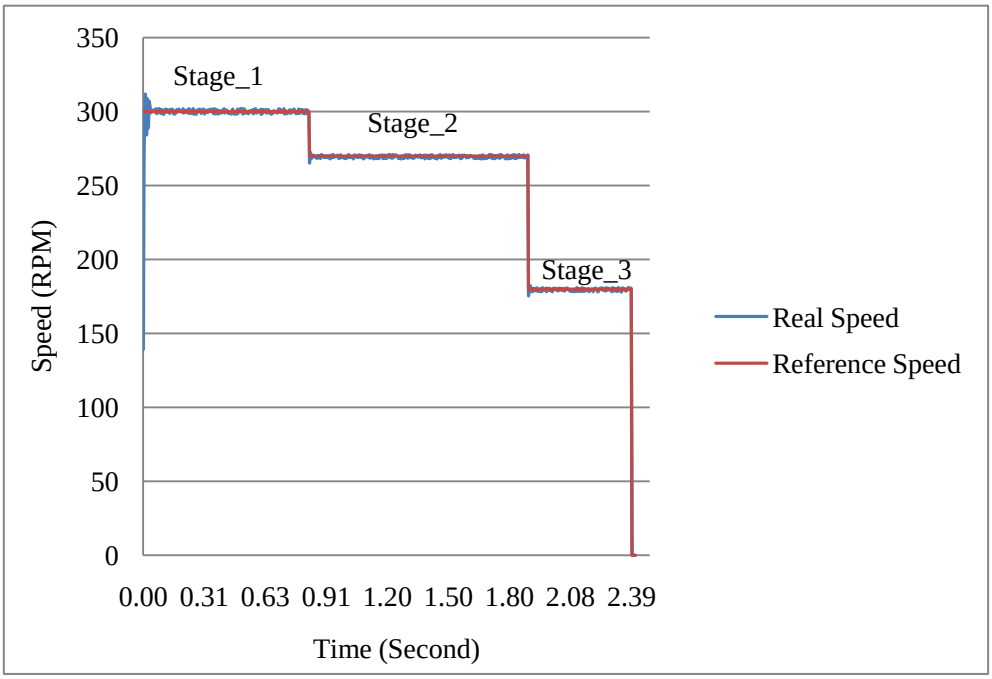

Figure 4.8. Result of varying speed at constant load

4.3.1.2 Experimental result of constant speed with varying loads

In this case, the shaft speed was set to a constant value at 300 RPM. The load was linearly changed from 0 to 30 lbs·ft. As it is shown in Figure 4.9, the overall tolerance band was maintained within 1.85%, which demonstrated that the controller gave a satisfying stable response to load variations.

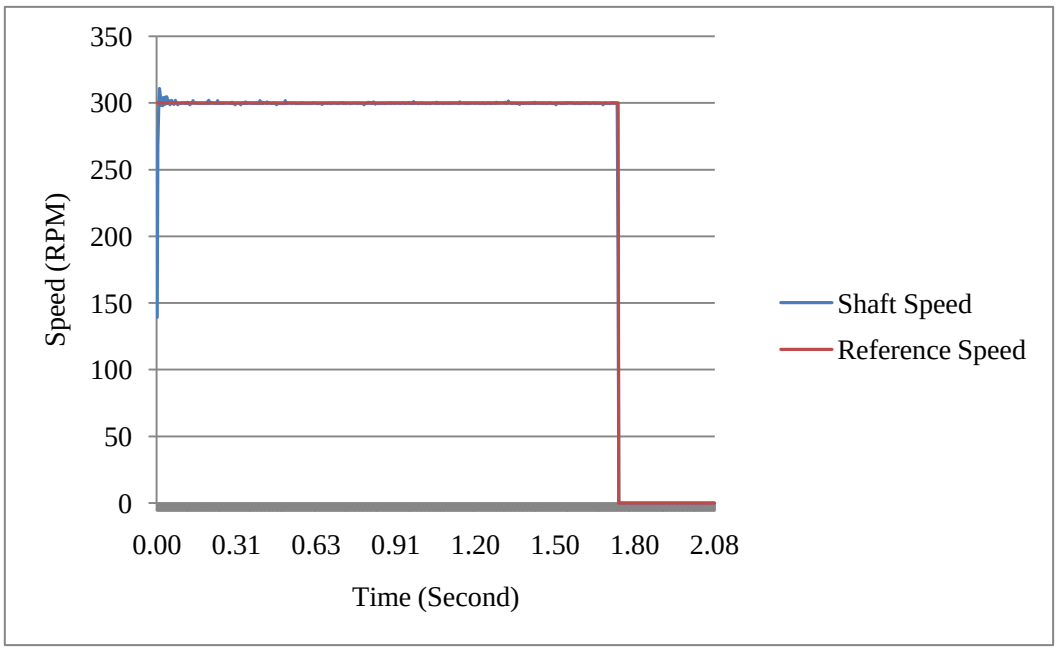

Figure 4.9. Result of varying load at constant shaft speed

4.3.2 Experimental results of speed control with fault occurrence

When taking into consideration of the information from vibration signals, kurtosis value and peak-to-peak value vary with the changes in bearing conditions. The input pairs used at different stages of the experiment are listed in Table 4.3. All these pairs originated from data presented in Table 3.1 in Appendix I.

With the original mapping result in Table 3.4 and Table 3.5,the experimental results with parameters in Table 4.3are shown in Figure 4.10. The result shows that the control system is sensitive to and can respond quickly to bearing condition changes reflected by, kurtosis values and peak-to-peak values. During the first stage, the bearing was healthy and the shaft speed was maintained at the set value. As the fault developed (reflected by a kurtosis value of 3.797 and PPV at 1.340, the shaft speed was reduced correspondingly to around 172 RPM. As the severity of the bearing defect increased (reflected by high kurtosis value of 21.005 and PPV of 13.060), the turbine came to a complete stop to protect the wind turbine test rig.

Table 4.3. Kurtosis value and peak-to-peak value pairs for experiments

Stage	Stage _1	Stage_2	Stage_3
Kurtosis	2.929	3.797	21.005
PPV	0.670	1.340	13.060

Table 4.4. Kurtosis value and PPV pairs for experiments from UO

Stage	Stage _1	Stage_2	Stage_3
Kurtosis	3.568	6.281	9.341
PPV	0.212	0.491	0.510

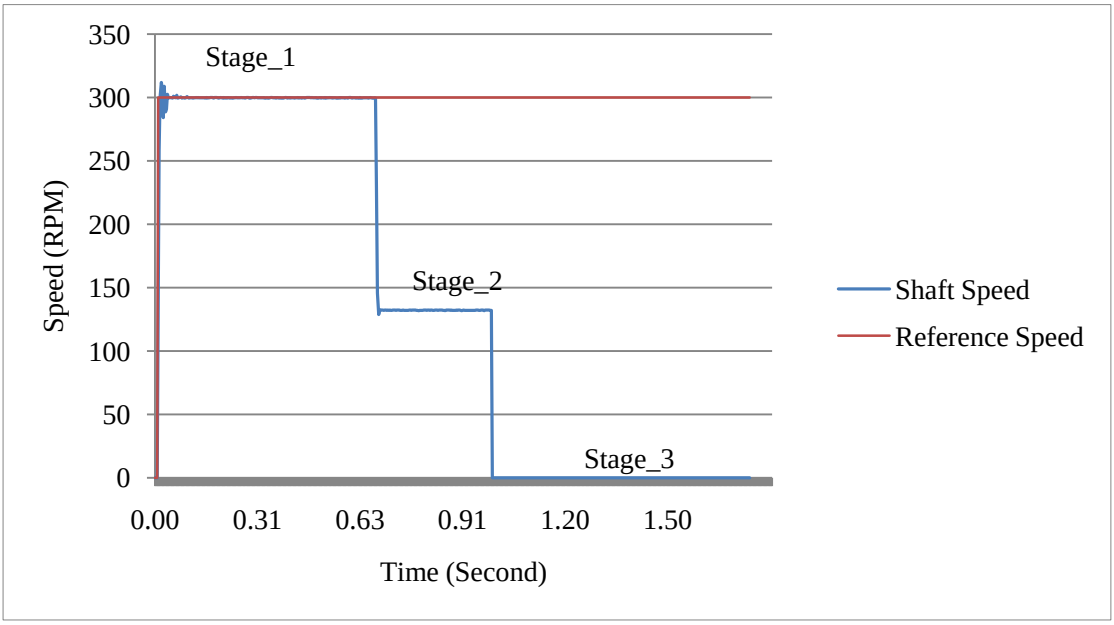

Figure 4.10. Test result with bearing condition changes (based on the data from the Case Western Reserve University)

If the self-tuning mechanism is removed, the fuzzy control system exhibits inappropriate response to bearing conditions. This can be illustrated using the data from the lab at the University of Ottawa (UO)shown in Table 4.4.

In this case, the set value for the shaft speed was also 300 RPM. The result is shown in Figure 4.11. There are three periods illustrated in the figure. During the first period,

speed was maintained at 300 RPM with the initial kurtosis value and the peak-to-peak value set to fuzzy zero. When kurtosis value and peak-to-peak value were set to the pair as presented underStage_1 in Table 4.4, the shaft speed dropped down slightly and maintained at around 295 RPM. When Stage_2 and Stage_3 pairs in Table 4.4were used, the shaft speed continued to drop, but no apparent difference can be observed between Stage_2 and Stage_3 settings.

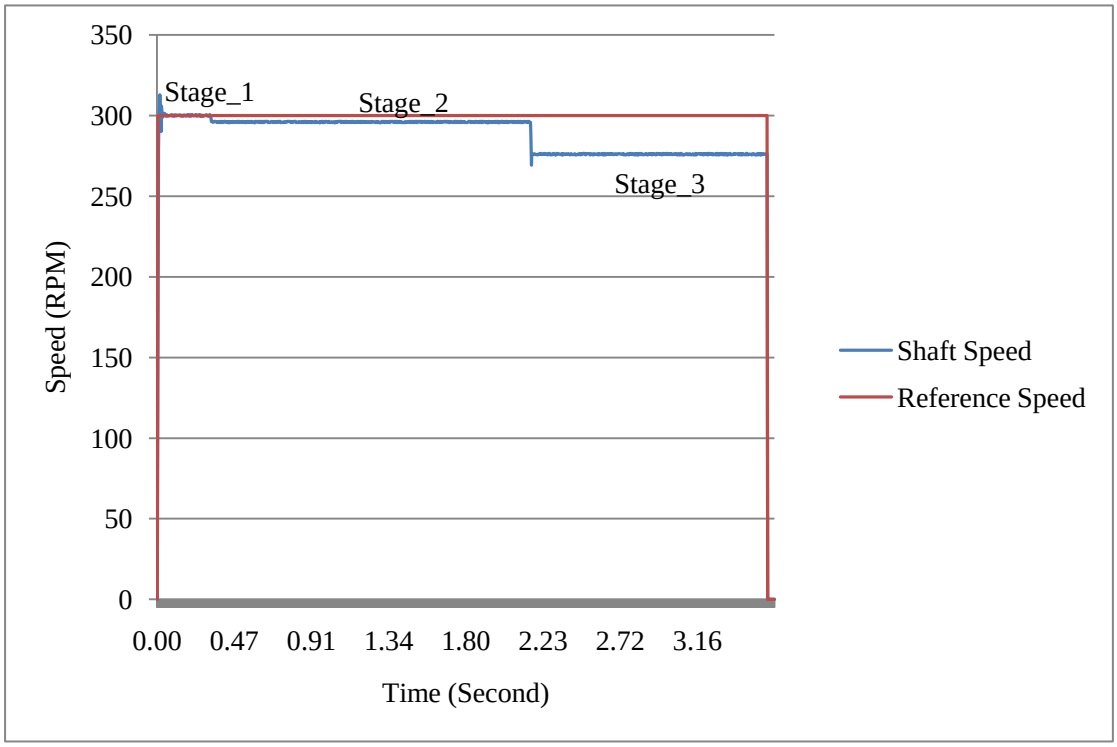

Figure 4.11. Result of experiment with OU bearing information without tuning

When the membership was tuned by the proposed tuning mechanism, the updated membership functions offered a better performance in detecting faults. The result is shown in Figure 4.12.

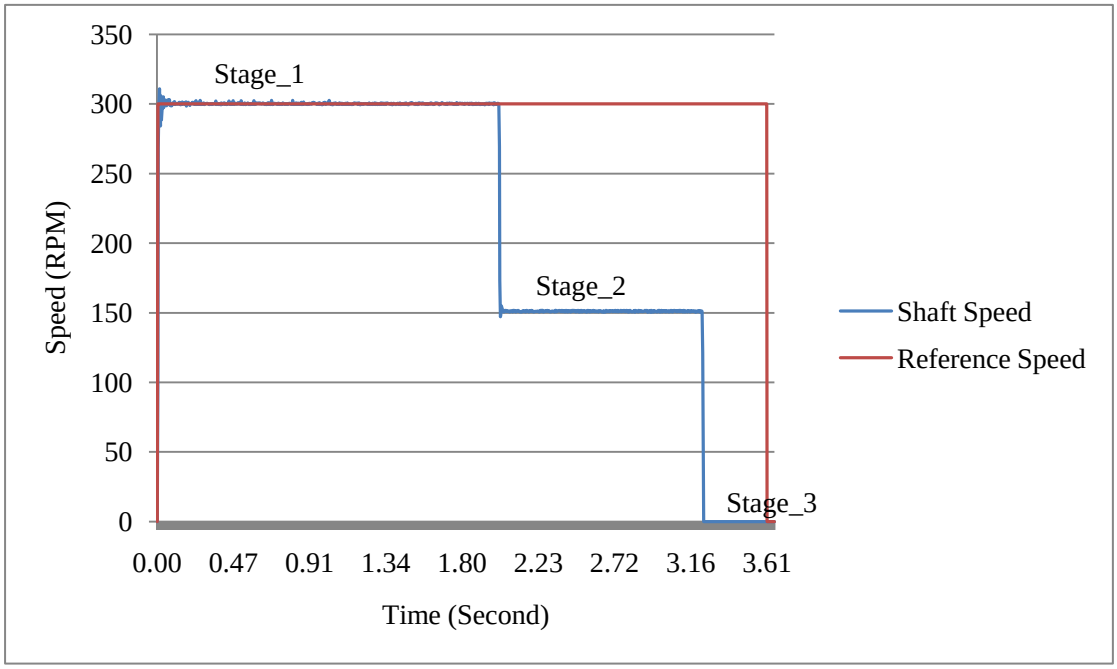

Figure 4.12. Results of experiment with OU bearing information with tuning

Initially, the kurtosis value and the peak-to-peak value were both set to fuzzy zero. The two values were then changed to the Stage_1 pair (i.e., 3.568 and 0.212, respectively) in Table 4.4. The shaft speed remained at 300 RPM, which was the set value. This is reasonable because such low kurtosis and PPV values indicate a healthy bearing condition. When the input pair takes the values of Stage_2 (i.e., kurtosis = 6.281 and PPV = 0.491) in Table 4.4, the shaft speed drops sharply to 150 RPM. After feeding the Stage_3 pair into the controller, the control mechanism considered that a severe defect occurred and accordingly stopped the shaft. These results are similar to those shown in Figure 4.10.

Chapter 5. Conclusions and Future Research

5.1 Conclusion

A fuzzy logic based self-tuning system for simultaneous bearing fault detection and shaft speed control has been developed. Our experimental results indicate:

1. The system performed very well at different shaft speeds with constant load. It can help to maintain the user-specified speed while the load changes dynamically.

2. With dual indicators and proper weight, the system can detect bearing fault and therefore provide guidance to shaft speed control.

3. This controller is able to adjust output speed in response to bearing conditions so as to protect the wind turbine test rig.

4. The implementation of the proposed self-tuning mechanism improves the adaptability of the proposed fuzzy system and hence enhances the control performance reflected by amount of speed adjustment responding to bearing severity.

5.2 Future Research

Further studies may be carried out in the following directions:

1. With this proposed control and monitoring platform, more fault detection information can be integrated and further control actions can be realized based on more sophisticated detection and control techniques. Further integration with other monitoring and control tasks of interest could broaden the multi-tasking capability of the system.

2. For the fault detection part, self-learning mechanism can be implemented in conjunction with more sophisticated fault detection techniques to strengthen its adaptability and functionality.

References

Alcala, R., Alcala-Fdez, J., and Herrera, F., 2007, A proposal for the genetic lateral tuning of linguistic fuzzy systems and its interaction with rule selection. *IEEE Transactions on Fuzzy Systems*, **15**(4), 616-635.

Alcala-Fdez, J., Alcala, R., and Herrera, F., 2011, A fuzzy association rule-based classification model for high-dimensional problems with genetic rule selection and lateral tuning. *IEEE Transactions on Fuzzy Systems*, **19**(5), 857-872.

Anh, H.P.H., and Ahn, K.K., 2011, Hybrid control of a pneumatic artificial muscle (PAM) robot arm using an inverse NARX fuzzy model. *Engineering Applications of Artificial Intelligence*, **24**(4), 697-716.

Antoni, J.,2006, The spectral kurtosis: a useful tool for characterizing non-stationary signals. *Mechanical Systems and Signal Processing*, **20**, 282-307.

Antoni, J., 2007, Fast computation of the kurtogram for the detection of transient faults. *Mechanical Systems and Signal Processing*, **21**(1), 108–124.

Antoni, J., and Randall, R.B., 2006, The spectral kurtosis: application to the vibratory surveillance and diagnostics of rotating machines. *Mechanical Systems and Signal Processing*, **20**(2), 308–331.

Barazane, L., Sicard, P., and Ouiguini, R., 2009, Cascade fuzzy variable structure control of induction motor based on the approach of fuzzy modeling of Ben-Ghalia. *International Journal of Systems Science*, **40**(3), 309-326.

Bououden, B., Chadli, M., Filali, S., and El Hajjaji, A., 2012, Fuzzy model based multivariable predictive control of a variable speed wind turbine: LMI approach.

Renewable Energy, **37**(1), 434-439.

Casillas, J., Cordon, O., Del Jesus, M.J., and Herrera, F., 2005, Genetic tuning of fuzzy rule deep structures preserving interpretability and its interaction with fuzzy rule set reduction. *IEEE Transactions on Fuzzy Systems*, **13**(1), 13-29.

Chang, W., Hwang, R., and Hsieh, J., 2003, A multivariable on-line adaptive PID controller using auto-tuning neurons. *Engineering Applications of Artificial Intelligence*, **16**(1), 57-63.

Chaturved, G.K., and Thomas, D.W., 1981, Adaptive noise cancelling and condition monitoring. *Journal of Sound and Vibration*, **76**(3), 391-405.

Choi, Y., and Kim, Y., 2007, Fault detection in a ball bearing system using minimum variance cepstrum. *Measurement Science and Technology*, **18**(5), 1433-1440.

Choy, F. K., Jia, W., Wu, R., 2009, Identification of bearing and gear tooth damage in a transmission system. *Tribology Transactions*, **52** (3), 303-309.

Ciang, C.C., Lee, J., and Bang, H., 2008, Structural health monitoring for a wind turbine system: a review of damage detection methods. *Measurement Science and Technology*, **19**(12), 1-20.

Combet, F., and Gelman, L., 2009, Optimal filtering of gear signals for early damage detection based on the spectral kurtosis. *Mechanical Systems and Signal Processing*, **23**(3), 652–668.

Dadone, A., and Dambrosio, L., 2003, Estimator based adaptive fuzzy logic control technique for a wind turbine–generator system. *Energy Conversion and Management*,

44(1), 135-153.

Dalgaard, E., Auken, E., and Larsen, J.J., 2012, Adaptive noise cancelling of multichannel magnetic resonance sounding signals. *Geophysical Journal International*, **191**(1), 88-100.

Dandil, B., 2009, Fuzzy neural network IP controller for robust position control of induction motor drive. *Expert Systems with Applications*, **36**(3), 4528-4534.

D ńz, B., Moniche, L., and Morillas, A., 2006, A fuzzy clustering approach to the key sectors of the Spanish economy. *Economic Systems Research*, **18**(3), 299-318.

Driankov, D., and Hellendoorn, H.,1996, *An Introduction to Fuzzy Control*, 2nd ed., (Berlin: Springer).

Elforjani, M., and Mba, D., 2010, Accelerated natural fault diagnosis in slow speed bearings with acoustic emission. *Engineering Fracture Mechanics*, **77**(1), 112-127.

Gacto, M.J., Alcala, R., and Herrera, F., 2010, Integration of an index to preserve the semantic interpretability in the multi objective evolutionary rule selection and tuning of linguistic fuzzy systems. *IEEE Transactions on Fuzzy Systems*, **18**(3), 515-531.

Gagne, G., Laroche, E., Piccin, O., and Gangloff, J., 2010, Active heart stabilization using adaptive noise cancelling techniques with gyroscopic actuation. *IEEE RAS & EMBS International Conference on Biomedical Robotics and Biomechatronics*, Tokyo, Japan, 802-807.

Girdhar, P., and Scheffer, C., 2004, *Practical Machinery Vibration Analysis and Predictive Maintenance*, 1st ed., (Burlington: Elsevier).

Gürocak.H.B., and de Sam Lazaro, A., 1994, A fine tuning method for fuzzy logic rule bases. *Fuzzy Sets and Systems*, **67**(2), 147-161.

Hajnayeb, A., Khadem, S.E., and Moradi, M.H., 2008, Design and implementation of an automatic condition-monitoring expert system for ball-bearing fault detection. *Industrial Lubrication and Tribology*, **60**(2), 93-100.

Hou, S., Li, Y., and Wang, Z., 2010, A resonance demodulation method based on harmonic wavelet transform for rolling bearing fault diagnosis. *Structural Health Monitoring*, **9**(4), 297-308.

Howell, M.N., and Best, M.C., 2000, On-line PID tuning for engine idle-speed control using continuous action reinforcement learning automata. *Control Engineering Practice*, **8**(2), 147-154.

Kandiban, R., and Arulmozhiyal, R., 2012, Speed control of BLDC motor using adaptive fuzzy PID controller. *Procedia Engineering*, **38**, 306-313.

Kankar, P.K., Sharma, S.C., and Harsha, S.P., 2011a, Fault diagnosis of ball bearings using continuous wavelet transform. *Applied Soft Computing Journal*, **11**(2), 2300-2312.

Kankar, P.K., Sharma, S.C., and Harsha, S.P., 2011b, Rolling element bearing fault diagnosis using wavelet transform. *Neurocomputing*, **74**(10), 1638-1645.

Karasakal, O., Guzelkaya, M., Eksin, I., and Yesil, E., 2011, An error-based on-line rule weight adjustment method for fuzzy PID controllers. *Expert Systems with Applications*, **38**(8), 10124-10132.

Lee, Y., Park, S., and Lee, M., 2006, Consider the generalized IMC-PID method for PID controller tuning of time-delay processes. *Hydrocarbon Processing*, 87-91.

Li, F., Meng, G., Ye, L., and Chen, P., 2008, Wavelet transform-based higher-order statistics for fault diagnosis in rolling element bearings. *Journal of Vibration and Control*, **14**(11), 1691-1709.

Li, Z., He, Z., Zi Y., and Chen, X., 2008, Bearing condition monitoring based on shock pulse method and improved redundant lifting scheme. *Mathematics and Computers in Simulation*, **79**(3), 318-338.

Li, M., and Liu, D., 2011, A novel adaptive self-tuned PID controller based on recurrent-wavelet-neural-network for PMSM speed servo drive system. *Procedia Engineering*, **15**, 282-287.

Liang, M., and Soltani Bozchalooi, I., 2010, An energy operator approach to joint application of amplitude and frequency-demodulations for bearing fault detection. *Mechanical Systems and Signal Processing*, **24**(5), 1473-1494.

Liu, Y., Guo, L., Wang, Q., An, G., Guo, M., and Lian, H., 2010, Application to induction motor faults diagnosis of the amplitude recovery method combined with FFT. *Mechanical Systems and Signal Processing*, **24**(8), 2961-2971.

Marichal, G.N., Artés, M., and García-Prada, J.C., 2011, An intelligent system for faulty-bearing detection based on vibration spectra. *Journal of Vibration and Control*, **17**(6), 931-942.

McFadden, P.D., and Smith, J.D., 1984, Vibration monitoring of rolling element

bearings by the high-frequency resonance technique: a review. *Tribology International*, **17**(1), 3-10.

Park, H., Oh, S., and Lee, S., 2002, Adaptive noise cancelling based on independent component analysis. *Electronics Letters*, **38**(15), 832-833.

Prabhakar, S., Mohanty, A.R., Sekhar, A.S., 2002, Application of discrete wavelet transform for detection of ball bearing race faults. *Tribology International*,**35** (12),793-800.

Precup, R., and Hellendoorn, H., 2011, A survey on industrial applications of fuzzy control. *Computers in Industry*, **62**(3), 213-226.

Qi, Y., and Meng, Q., 2012, The application of fuzzy PID control in pitch wind turbine. *Energy Procedia*, **16**, 1635-1641.

Rai, V.K., and Mohanty, A.R., 2007, Bearing fault diagnosis using FFT of intrinsic mode functions in Hilbert-Huang transform. *Mechanical Systems and Signal Processing*, **21**(6), 2607-2615.

Rezaei, A., Dadouche, A., Wickramasinghe, V., and Dmochowski, W., 2011, A comparison study between acoustic sensors for bearing fault detection under different speed and load using a variety of signal processing techniques. *Tribology Transactions*, **54**(2), 179-186.

Saad, N., and Arrofiq, M., 2012, A PLC-based modified-fuzzy controller for PWM-driven induction motor drive with constant V/Hz ratio control. *Robotics and Computer Integrated Manufacturing*, **28**(2), 95-112.

Sanz, J.A., Fernández, A., Bustince, H., and Herrera, F., 2012, Improving the performance of fuzzy rule-based classification systems with interval-valued fuzzy sets and genetic amplitude tuning. *Information Sciences*, **180**(19), 3674-3685.

Sanz, J., Fernández, A., Bustince, H., and Herrera, F., 2011, A genetic tuning to improve the performance of fuzzy rule-based classification systems with interval-valued fuzzy sets: degree of ignorance and lateral position. *International Journal of Approximate Reasoning*, **52**(6), 751-766.

Sanz, J., Fernández, A., Bustince, H., and Herrera, F., 2010, A genetic algorithm for tuning fuzzy rule-based classification systems with interval-valued fuzzy sets. *International Conference on Fuzzy Systems*, Barcelona, Spain, 1-3.

Senjyu, T., Sakamoto, R., Kaneko, T., Yona, A., and Funabashi, T., 2008, Output power leveling of wind farm using pitch-angle control with fuzzy neural network. *Electric Power Components and Systems*, **36**(10), 1048-1066.

Sheen, Y.T., 2009, On the study of applying Morlet wavelet to the Hilbert transform for the envelope detection of bearing vibrations. *Mechanical Systems and Signal Processing*, **23**(5), 1518-1527.

Shin, H., and Park, J., 2012, Anti-windup PID controller with integral state predictor for variable-speed motor drives. *IEEE Transactions on Industrial Electronics*, **59**(3), 1509-1516.

Singh, G.K., and Al Kazzaz, S.A.S., 2009, Isolation and identification of dry bearing faults in induction machine using wavelet transform. *Tribology International*, **42**(6), 849-861.

Smimou, K., Bector, C.R., and Jacoby, G., 2008, Portfolio selection subject to experts' judgments. *International Review of Financial Analysis*, **17**(5), 1036-1054.

Subramanyam, M.V., Satya Prasad, K., and Gopi Krishna Rao, P.V., 2012, Robust control of steam turbine system speed using improved IMC tuned PID controller. *Procedia Engineering*, **38**, 1450-1456.

Sugumaran, V., and Ramachandran, K.I., 2011, Effect of number of features on classification of roller bearing faults using SVM and PSVM. *Expert Systems with Applications*, **38**(4), 4088-4096.

Taha, M., Noureldin, A., Lucero, J., and Baca, T., 2006, Wavelet transform for structural health monitoring: a compendium of uses and features. *Structural Health Monitoring*, **5**(3), 267-295.

Tan, K.K., Lee, T.H., and Jiang, X., 2001, On-line relay identification, assessment and tuning of PID controller. *Journal of Process Control*, **11**(5), 483-496.

Tandon, N., and Choudhury, A., 1999, A review of vibration and acoustic measurement methods for the detection of defects in rolling element bearings. *Tribology International*, **32**(8), 469-480.

Wang, H., Chen P., 2011, Fuzzy diagnosis method for rotating machinery in variable rotating speed. *IEEE Sensors Journal*, **11**(1), 23-34.

Wang, Y., and Liang, M., 2012, Identification of multiple transient faults based on the adaptive spectral kurtosis method. *Journal of Sound and Vibration*, **331**(2), 470-486.

Wang, Y., and Liang, M., 2011, An adaptive SK technique and its application for fault

detection of rolling element bearings. *Mechanical Systems and Signal Processing*, **25**(5), 1750-1764.

Widrow, B., Glover, J.R. Jr., McCool, J.M., Kaunitz, J., Williams, C.S., Hearn, R.H., Zeidler, J.R., Dong, E. Jr., and Goodlin, R.C., 1975, Adaptive noise cancelling: principles and applications. *Proceedings of the IEEE*, **63**(12), 1692-1716.

Xiao, Y., 2010, A novel optimum power fuzzy control strategy for doubly-fed wind turbine. *IEEE International Conference on Control and Automation*, Xiamen, China, 165-170.

Yang, Z., Zhang, B., Zhang, J., and Wang, C., 2011, Research on semi-active control of high-speed railway vehicle based on neural network-PID control. *International Conference on Natural Computation*, Shanghai, China, **2**, 673-676.

Yang, Z., Zhang, Z., Chen, Z., and Zhang, B., 2011, Semi-active control of high-speed trains based on fuzzy PID control. *Procedia Engineering*, **15**, 521-525.

Zhang, J., Ni, G., and Zhang, J., 2006, Neural network based PID control on NC milling process with high-speed. *International Technology and Innovation Conference*, Hangzhou, China, 551-555.

Zhu, K., Wong, Y.S., and Hong, G.S., 2009, Wavelet analysis of sensor signals for tool condition monitoring: a review and some new results. *International Journal of Machine Tools and Manufacture*, **49**(7-8), 537-553.

Appendix I Kurtosis and PPV Values Tables

Table 3.1. Kurtosis and PPV values of the Case Western Reserve University bearing data center

No.	Data file name	Kurtosis	PPV
	Healthy Bearing		
01	bearing-no-0-1797-12k[1)]	2.765	0.600
02	bearing-no-1-1772-12k	2.929	0.670
03	bearing-no-2-1750-12k	2.925	0.690
04	bearing-no-3-1730-12k	2.956	0.590
	OR-FE[2)]		
05	bearing-or-007-0-1797[3)]	12.328	6.684
06	bearing-or-007-1-1772	15.188	5.797
07	bearing-or-007-2-1750	15.788	6.154
08	bearing-or-007-3-1730	15.279	6.063
09	bearing-or-014-0-1797	7.764	9.841
10	bearing-or-021-0-1797	8.785	10.585
	OR-DE[4)]		
11	bearing-or-007-0-1797[5)]	7.650	7.040
12	bearing-or-007-1-1772	7.594	6.120
13	bearing-or-007-2-1750	7.852	6.180
14	bearing-or-007-3-1730	7.963	6.240
15	bearing-or-014-0-1797	3.057	1.100

16	bearing-or-014-1-1772	2.941	0.800
17	bearing-or-014-2-1750	3.025	0.890
18	bearing-or-014-3-1730	3.797	1.340
19	bearing-or-021-0-1797	21.005	13.060
20	bearing-or-021-1-1772	21.972	12.320
21	bearing-or-021-2-1750	23.161	13.300
22	bearing-or-021-3-1730	23.542	13.300
	IR-FE[5)]		
23	bearing-ir-007-0-1797	7.293	3.776
24	bearing-ir-007-1-1772	6.103	2.921
25	bearing-ir-007-2-1750	5.903	2.968
26	bearing-ir-007-3-1730	5.317	2.949
27	bearing-ir-014-0-1797	5.500	2.226
28	bearing-ir-014-1-1772	5.641	1.776
29	bearing-ir-014-3-1730	5.523	1.731
30	bearing-ir-021-0-1797	7.093	4.225
31	bearing-ir-021-1-1772	6.481	3.395
32	bearing-ir-021-2-1750	5.961	4.303
33	bearing-ir-021-3-1730	5.885	3.292

Note: 1) bearing-no-0-1797-12kmeans bearing data, no fault, 1 horsepower, 1772 rpm shaft speed, and sampling frequency is 12,000 Hz;

2) OR-FE means outer race fault of the bearing at the fan end;

3) bearing-or-007-0-1797 represents bearing fault of outer race, fault size is 0.007" in diameter, zero horsepower (no load) at a shaft speed of 1797 rpm;

4) OR-DE indicates that the bearing at the drive (motor) end has an outer race fault; and

5) IR-FE stands for inner race fault of the bearing at the fan end.

Table 3.2. Kurtosis and PPV values of the University of Ottawa data (5/8" shaft)

Condition[1)]	Kurtosis	PPV
B00 H	3.568	0.212
B01 IR	9.341	0.510
B02 OR	6.281	0.491
B03 H	3.240	0.161
B04 IR	10.652	0.735
B05 OR	9.058	0.681
B06 H	5.426	0.310
B07 IR	44.200	1.763
B08 OR	10.892	1.599
B18 Faulty[2)]	8.750	0.190
B19 Faulty	6.146	0.264

Note: 1) Bxx: file number, one faulty bearing at drive end with various loads, at the speed of 500rpm without gearbox connected, H: Healthy, IR: Inner -race fault, OR: Outer-race fault; and 2) B18 and B19: Two faulty bearings without gear vibration.

Appendix II COM Inference Process

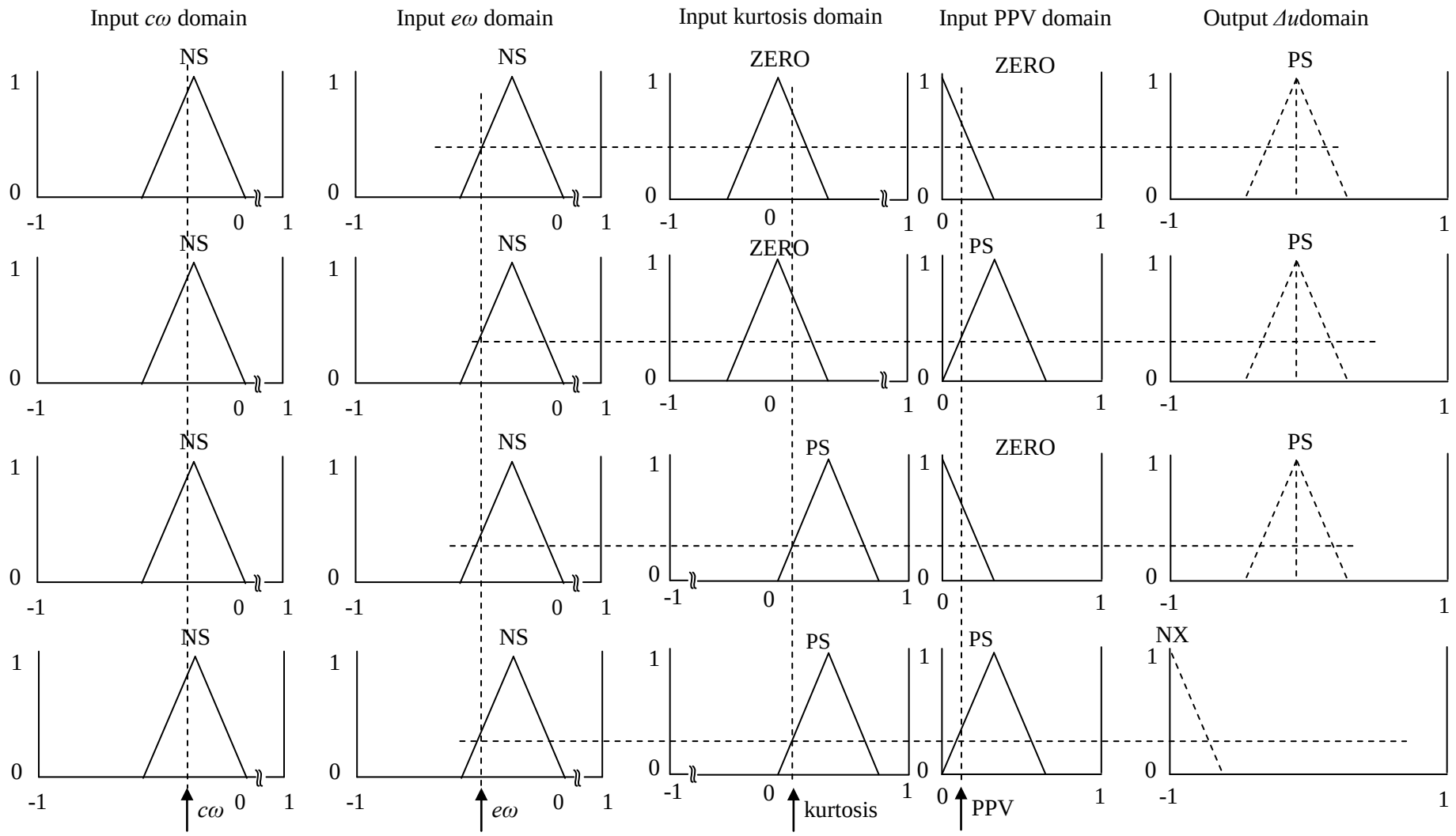

Figure 3.11.COM inference process

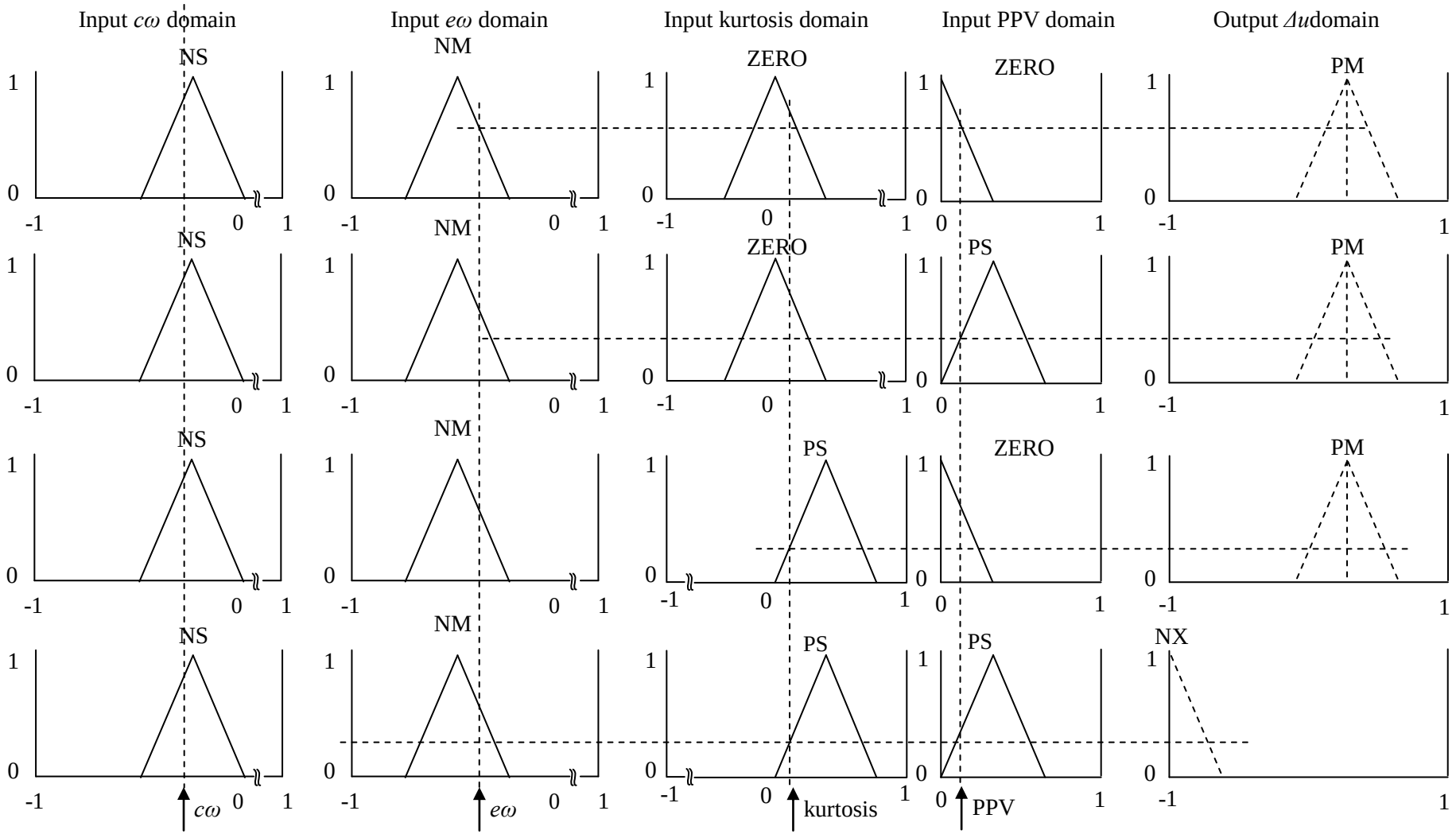

Figure 3.12.COM inference process (continued)

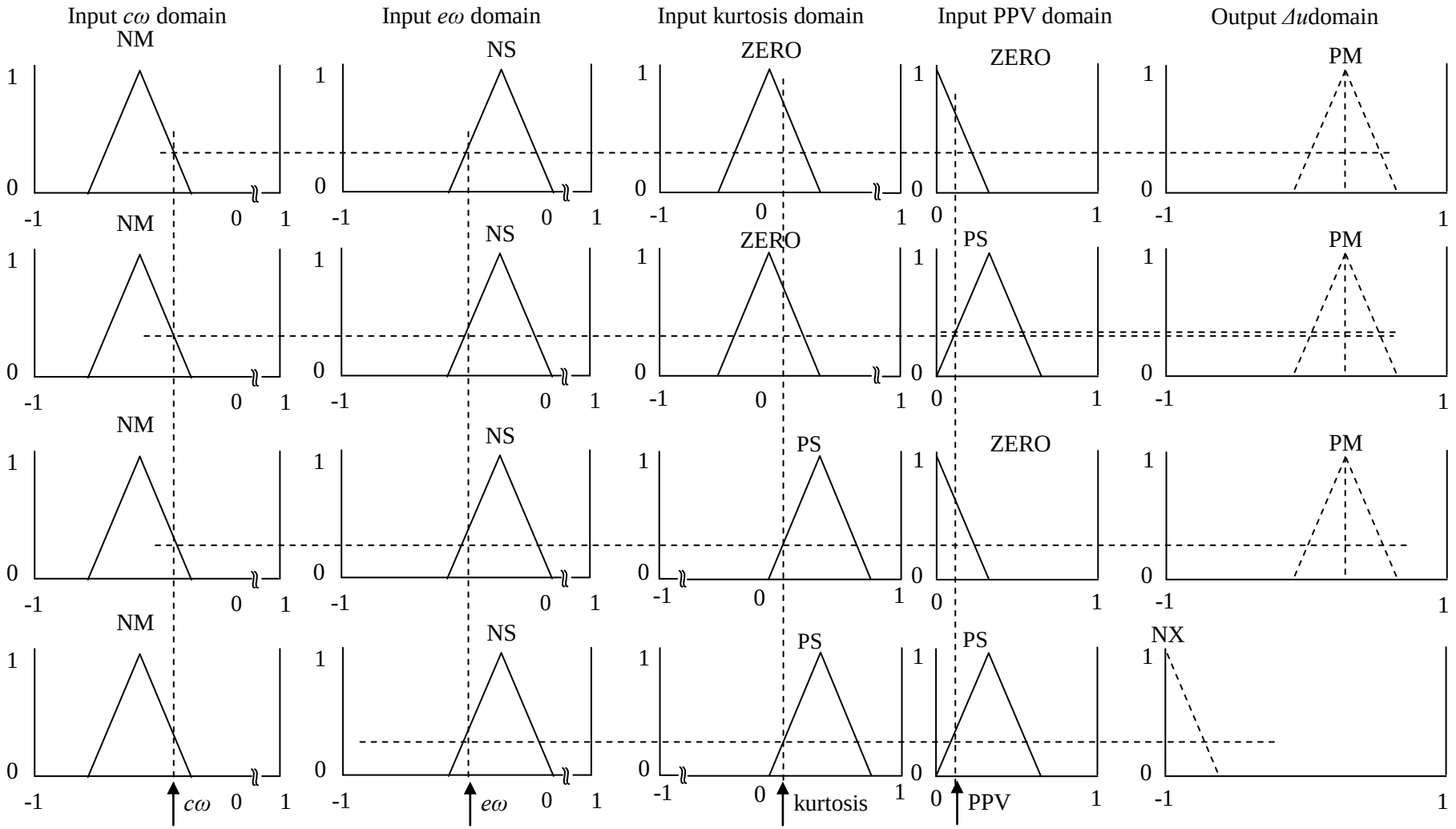

Figure 3.13.COM inference process (continued)

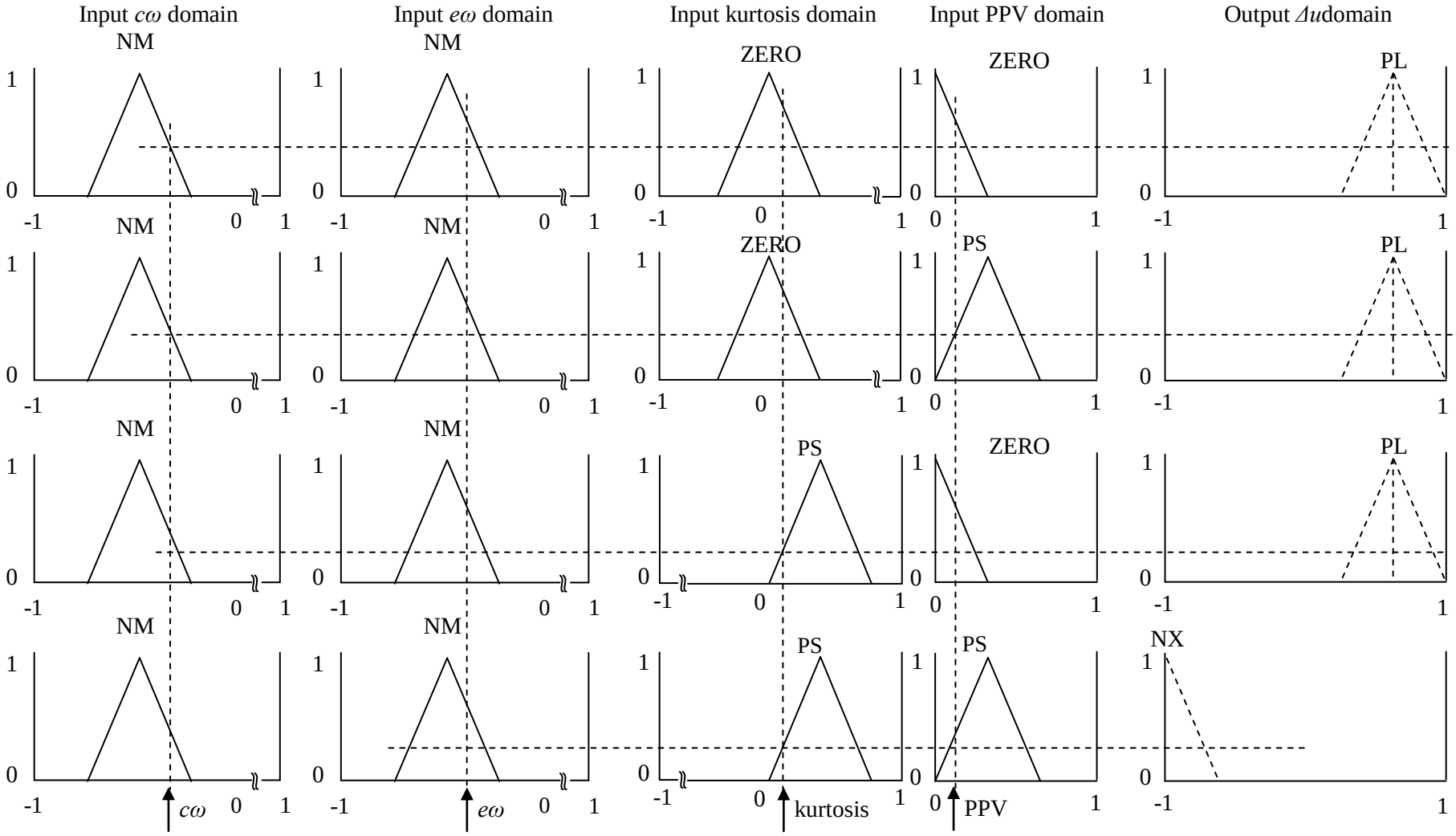

Figure 3.14.COM inference process (continued)

Appendix III Programs for Wireless Modules

1. Wireless module - master terminal

```
% wireless module - master terminal
%initialization
int comData = 0;
char string[3] ;
int p = 0;
int oldDigiValue = 'L';
int mark = 1;
const int vfdPin = 5;
const int digiOutPin = 8;
int analogValue = 0;

int numOfImpulse = 0;
unsigned long oldTime = 0;
int motorFrequency = 0;

void setup()
{
    Serial.begin(9600);
    pinMode(vfdPin, OUTPUT);
    pinMode(digiOutPin, OUTPUT);
    digitalWrite(vfdPin,LOW);
    digitalWrite(digiOutPin,LOW);
    attachInterrupt(0, tachoCount, RISING);//interrupt0 = pin2
}
void loop()
{
      if(Serial.available() > 10)
      {
```

```
        while(mark == 1)
        {
                comData = Serial.read();
                if((comData >= '0') && (comData <= '9'))
                {
                    string[p] = comData;
                    p++;
                }

                if((comData == 'H') || (comData == 'L'))
                {
                     analogValue = atoi(string);

                    //clear the string and break out
                        for(int c = 0; c<p; c++)
                        {
                            string[c] = 0;
                        }

                    p = 0;
                    mark = 0;
                }
        }
  }

if((analogValue>0) && (analogValue<=255))
{
   analogWrite(vfdPin,analogValue);
}

if ( comData != oldDigiValue)
```

```
    {
        if(comData == 'H')
        {
            digitalWrite(digiOutPin,HIGH);
            //Serial.println('H');
            oldDigiValue = 'H';
        }

        if(comData == 'L')
        {
            digitalWrite(digiOutPin,LOW);
            //Serial.println('L');
            oldDigiValue = 'L';
        }
    }
    mark = 1;
}

%Counter definition
void tachoCount()
{
     numOfImpulse++;
     if (numOfImpulse == 1024)
     {
        int time = millis()-oldTime;
        motorFrequency = 10240/time;
        //Serial.println(lowByte(motorFrequency));
        Serial.write(motorFrequency);
        delay(2);
        numOfImpulse = 0;
        oldTime = millis();
```

```
      }
}
```

2. Wireless module - slave terminal

```
% wireless module - slave terminal
% Initialization
int analogInPin = 0;
const int digiInPin = 8;
int oldDigiState = 0;

const int digiOutPin = 5;
unsigned int tachometer = 0;
unsigned int oldTachometer = 1;

void setup()
{
   Serial.begin(9600);
   pinMode(digiInPin,INPUT);
   pinMode(digiOutPin,OUTPUT);
   digitalWrite(digiOutPin,LOW);
}

%Analog data function
void loop()
{
  int sensorValue = map(analogRead(analogInPin),0,1023,0,255); //read analog input and
map the value into 8bit
Serial.print('S'); // data start
  delay(2);
  Serial.print(sensorValue,DEC); // print the value of analog input
  delay(2);
```

```
// check the digital io status and if the status changes then print out the value.
    if( digitalRead(digiInPin) == 1)
    {
       delay(2);// debounce
       if( digitalRead(digiInPin) == 1)
       {
          Serial.print('H');
       }
    }

    if( digitalRead(digiInPin) == 0)
    {
       delay(2);// debounce
       if( digitalRead(digiInPin) == 0)
       {
          Serial.print('L');
       }
    }
    delay(1);
//receive tachometer reading (this part should be written
//into digiread part, for untone the tachometer out put)

     if(Serial.available() >0)
     {
          tachometer = Serial.read()*100;

          if(tachometer != oldTachometer)
          {
             if(tachometer != 0)
```

```
            {
              tone(digiOutPin,tachometer);
              //Serial.println(tachometer);
            }
            if(tachometer == 0)
            {
              noTone(digiOutPin);
              digitalWrite(digiOutPin,LOW);
            }
          oldTachometer = tachometer;
          }
      }
}
}
```